Journal of
Nanotheranostics

MDPI

Review

Activation Strategies in Image-Guided Nanotherapeutic Delivery

Seok Ki Choi [1,2]

[1] Michigan Nanotechnology Institute for Medicine and Biological Sciences, University of Michigan Medical School, Ann Arbor, MI 48109, USA; skchoi@umich.edu
[2] Department of Internal Medicine, University of Michigan Medical School, Ann Arbor, MI 48109, USA

Academic Editor: Dong-Hyun Kim
Received: 27 October 2020; Accepted: 25 November 2020; Published: 30 November 2020

Abstract: Therapeutic nanomaterials serve as an important platform for drug delivery under image guidance. Despite significant growth and broad applications, their design specifics remain a subject of continued interest primarily due to multifunctional factors involved, ranging from nanomaterial properties, imaging modalities, and therapeutic agents to activation strategies. This review article summarizes key findings on their design characteristics with a particular interest in strategies developed for therapeutic activation (release). First, their activation can be controlled using either an endogenous factor including low pH and glutathione or an external stimulation by light, ultrasound, or electromagnetic field. The former is passively controlled from a spatiotemporal aspect compared to the latter, which is otherwise actively controlled through drug linker photolysis, nanomaterial disassembly, or gate opening. Second, light stimulation serves a most notable strategy due to its essential role in controlled drug release, photothermal activation (hyperthermia), and photodynamic production of reactive oxygen species (ROS). Third, some of those activation strategies that rely on ultrasound, photothermal, photoacoustic, magnetic field, or X-ray radiation are dually functional due to their role in imaging modalities. In summary, this review article presents recent advances and new insights that pertain to nanotherapeutic delivery systems. It also addresses their technical limitations associated with tissue penetration (light), spatial resolution (ultrasound, hyperthermia), and occurrence of cellular resistance (ROS).

Keywords: nanotherapeutics; image-guided systems; therapeutic activation; controlled release

1. Introduction

Over recent decades, we have seen a rapid growth in and significant contribution by nanoscale therapeutic systems in image-guided delivery [1]. These systems utilize an integrative approach that combines both imaging and delivery functions in a single nanoscale entity. Their design is composed of three complementary modules that include an imaging probe, a therapeutic component, and a nanomaterial platform. Their imaging function plays a fundamental role in detecting and tracking the nanotherapeutic system following its administration (Figure 1). This helps to identify whether it is well distributed at its targeted site from a pharmacokinetic perspective and thus to determine an optimal timing for its therapeutic activation. Its therapeutic module is achieved with many strategies collectively by drug release [2–5], photothermal activation [6], photodynamic activation [7,8], or the combination of these. Nanomaterial platforms are more variable in the range of their structure and function as illustrated in dendrimer polymers [9–11], upconversion nanocrystals (UCN) [12–14], metal-organic frameworks [15], magnetic nanoparticles [16], and hollow nanostructures [17]. This modular approach employed in nanotherapeutic design offers a combinatorial convenience and broad applicability in various therapeutic areas and personalized medicine [1].

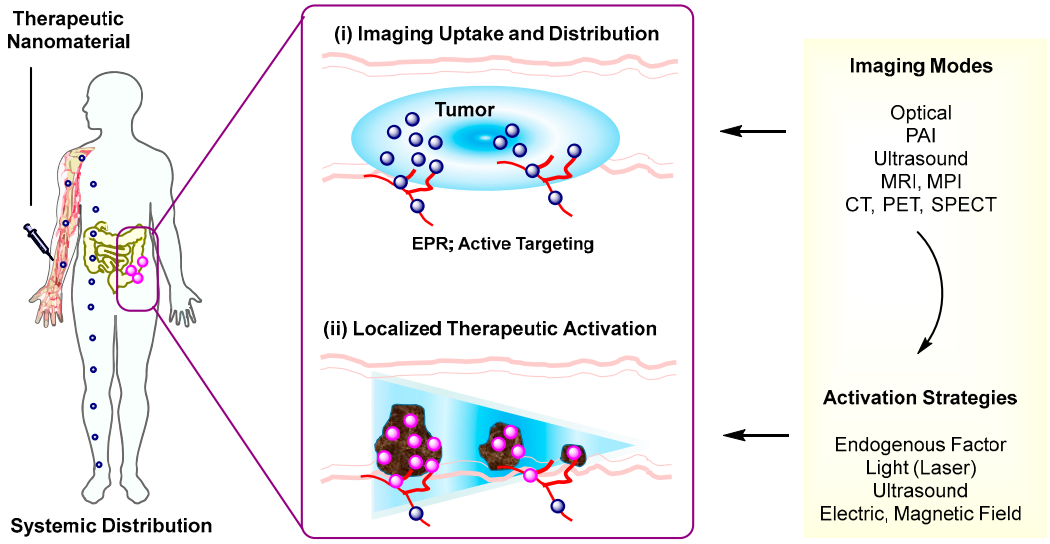

Figure 1. A schematic for image-guided nanotherapeutic delivery in tumors. A therapeutic nanomaterial is taken up in a diseased tissue via passive infiltration through leaky blood vessels or active biomarker targeting, imaged and therapeutically activated by endogenous factors or external stimulation.

In this article, therapeutic strategies are presented with regard to their activation mechanisms. Activation strategies which are covered here involve stimulations by either endogenous factors (pH, glutathione) [18,19] or external stimuli including light [2–5], ultrasound (US) [20–22], alternating magnetic field [4,16], or electric field [23]. These stimuli provide various mechanisms applicable for therapeutic activation including drug release that occurs through linker cleavage, nanomaterial disassembly, or gate opening. These strategies are described along with design factors involved in the selection and integration of imaging probes, payloads, and linkers to nanomaterials. Of particular focus is their individual role in therapeutic activation that occurs via stimulus-controlled linker cleavage, nanomaterial degradation, or induction of porosity.

Another important aspect described here relates to how therapeutic strategies are integrated with imaging modalities. For this purpose, delivery systems are to be introduced briefly for their imaging capability, which is achieved with ultrasound (US), magnetic resonance imaging (MRI), magnetic particle imaging (MPI), thermal imaging, photoacoustic imaging (PAI), X-ray computed tomography (CT), γ-ray positron emission tomography (PET), or single photon-emission computerized tomography (SPECT). It should be noted that these imaging methods have already been reviewed individually and comprehensively in several excellent articles [24–33], including those focused on optical [34], magnetic resonance [35], magnetic particle [32,33], photothermal [36], photoacoustic [37], and ultrasound [38].

Briefly, nanoscale systems are engineered for image-guided delivery through modular assembly. They are variable in modular principles, design characteristics, and activation strategies. Identifying a strategy for most optimal therapeutic efficacy remains an objective of significant interest [39]. This article offers new insights learned from recent advances in image-guided systems.

2. Therapeutic Activation by Endogenous Factors

2.1. Low pH

Cells provide several stimulating conditions applicable for controlled drug release. Some of these relate to low pH conditions in subcellular endosomes (pH 5.0–6.0) [40] and lysosomes [41,42] where nanomaterials initially reside after intracellular uptake through receptor-mediated endocytosis [43,44]. Similarly, acid-mediated release is reported to occur at extracellular matrices in tumors because they are more acidic than normal tissues [18]. This release strategy controlled by lowered pH has been used frequently in delivery systems. Some of its mechanistic basis is attributed to acid-catalyzed

linker hydrolysis [3] or degradation of acid-susceptible nanomaterials that include metal-organic frameworks [45], nanogels [35], and mesoporous silica oxide ($mSiO_2$) [46].

Figure 2 shows representative delivery systems based on pH-mediated therapeutic release. These include single-walled carbon nanotubes (SWNT) [43] designed for endosomal release of its cisplatin (IV) prodrug [3] (Figure 2A) and bortezomib-loaded polydopamine nanoparticulates [47] in which bortezomib linked through a boronic acid–catechol bonding is demonstrated for faster release at pH 5.4 than 7.4 (Figure 2B). The schematic in Figure 2D illustrates polymer micelles designed for extracellular activation catalyzed by acidic pH or proteinases [18]. This endogenous control is likewise applied in the release of doxorubicin loaded in acid-labile nanogels [35] or on the surface of iron oxide nanoparticles (IONP; Fe_3O_4) [48]. Delivery systems based on such magnetic nanomaterials as IONP allow MRI-guided drug delivery [35,48]. Another system controlled by low pH is porous $mSiO_2$ applied in the delivery of camptothecin, an anticancer drug that inhibits topoisomerase I in the nucleus [46]. Here, the drug molecule loaded in the porous shell layer of $mSiO_2$ is released when the silica layer is degraded in acidic subcellular compartments.

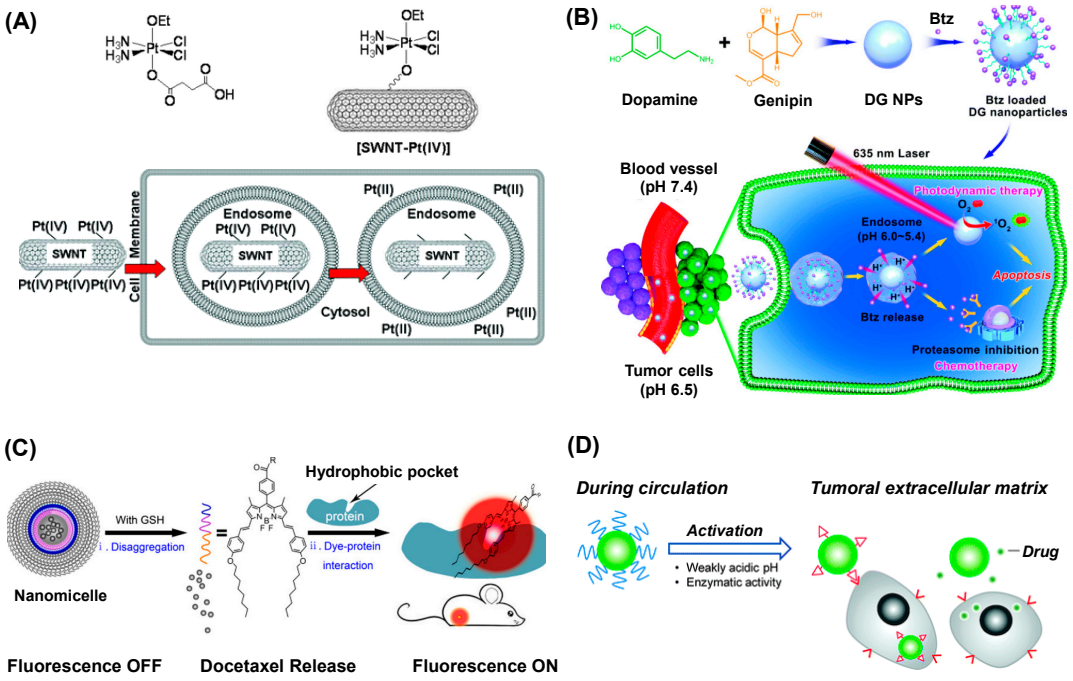

Figure 2. Representative strategies of therapeutic release by endogenous factors. (**A**) Single-walled carbon nanotube (SWNT) carrying a cisplatin (IV) prodrug, and its activation at endosomes where lowered pH facilitates reductive release of platinum (II) complex [43]. Reproduced with permission, Copyright 2007, American Chemical Society. (**B**) Bortezomib (Btz)-loaded polydopamine nanoparticle designed for pH-mediated drug release in combination with photodynamic therapy [47]. Reproduced with permission, Copyright 2019, Royal Society of Chemistry. (**C**) Docetaxel-loaded nanomicelle for fluorescence-guided tumor imaging and glutathione (GSH)-mediated drug release [49]. Reproduced with permission, Copyright 2016, American Chemical Society. (**D**) pH-responsive polymer micelles designed for extracellular activation triggered by acidic pH or proteinases in a tumor microenvironment [18]. Reproduced with permission, Copyright 2009, American Chemical Society.

2.2. Glutathione (GSH)

Cellular cytosols contain glutathione (GSH) at higher levels (2–10 mM) than the extracellular side [19]. This differential GSH expression serves as a trigger for facilitated intracellular release which occurs through a thiol (GSH)-disulfide exchange [50]. Release systems controlled by GSH are composed of disulfide drug linkers [50], reducible prodrugs or nanomaterials [49,51] made with

disulfide building blocks. Figure 2A,C each illustrate such release that includes a cisplatin (IV) prodrug loaded on SWNT which undergoes reductive activation to a platinum (II) species [43] and docetaxel release from degradable polymer micelles made of GSH-cleavable poly(ethylene glycol) (PEG) [49]. The latter micelle system is of relevance to image-guided drug delivery due to its ability for induction of fluorescence by a boron dipyrromethene (BODIPY) derivative that serves as a fluorescent probe when it is co-released with docetaxel.

Other pathophysiological conditions play a significant role in therapeutic activation as well. These are related with upregulated redox enzymes [52,53] and tumor hypoxia (low oxygen) [54]. Each of these is exploitable for prodrug activation or release as reported in prodrugs based on SN38 [53], naloxone [52], and Pt [43,55]. Another condition involves matrix metalloproteinase [56–58], a hydrolytic enzyme upregulated at tumors which is applicable for catalytic linker cleavage. It plays a role in the tumor-targeted delivery of methotrexate carried by dendrimer [56,57] or hyaluronic acid polymer [58]. In short, though passively controlled, drug release that occurs under endogenous conditions constitutes one of principal strategies explored in delivery systems.

3. Photocontrolled Therapeutic Release

Light stimulation serves as one of the important strategies that allow an active control in drug release [5,39]. It occurs via linker photolysis, nanomaterial disassembly [59–67], and pore gating [68–74]. It shows a higher degree of spatiotemporal resolution [3,75–77] than other external strategies stimulated by ultrasound or magnetic field [13,78]. Collectively, this accounts for its relatively higher precision in imaging and therapeutic activation [9,79]. However, it is notable that despite its benefits in spatial resolution and greater photochemical selectivity, light irradiation suffers from relatively lower tissue penetration, light scattering, and absorption by non-targeted biological molecules and tissues, each contributing to reducing its efficiency for drug activation [80].

3.1. Linker Photolysis

Release controlled by linker photolysis involves drug conjugation through a photocleavable linker made of *o*-nitrobenzyl (ONB) [11,81,82], thioacetal ONB [9,79], coumarin [51,83,84], quinolone [85,86], pyrene [87], acridin-9-methanol [88], or *N*-methyl-4-picolinium [89]. Figure 3 illustrates two linker systems made of either gold nanoparticle (AuNP) (Figure 3A) [81] or poly(amidoamine) (PAMAM) dendrimer (Figure 3B) [10], each carrying ONB linked 5-fluorouracil (5-FU) or ciprofloxacin, respectively. Upon exposure to long wavelength UV (365 nm), linker photolysis occurs, leading to rapid drug release. This also occurs consistently in cell studies in which 5-FU release results in induction of cytotoxicity in MCF-7 tumor cells (Figure 3A) as does ciprofloxacin in induction of antibacterial activity against *Escherichia coli* (Figure 3B). This release strategy is broadly applicable to various payloads from anticancer drugs (doxorubicin [9,11,14,90], methotrexate [91,92], 5-fluorouracil [81,83,89], paclitaxel [93], camptothecin [94], chlorambucil [84,87,95], platinum prodrug [96–98]), antibacterial ciprofloxacin [10,99,100], and biomolecules (DNA [101], oligonucleotide [102,103], Cas9-sgRNA [104]) to gas molecules (CO [105], NO [106–109], SO_2 [110], H_2S [111,112]).

Selecting light wavelengths that are optimal for linker photolysis is dependent on specific photophysical properties defined by linkers. This is illustrated with UV-cleavable ONB [11,81,82], visible light-cleavable coumarin [51,83,84], and near IR (NIR)-responsive cyanine [113,114]. However, linker integration with UCN opens an indirect route for NIR-triggered linker photolysis due to UCN luminescent emission at the UV and visible region upon irradiation at 980 nm [9,14,90]. This concept is illustrated in Figure 3 with UCN-based delivery systems designed for doxorubicin (Figure 3C) [14] or hydrogen sulfide (Figure 3D) [111], each linked through ONB to the UCN shell layer. Thus, NIR irradiation at 980 nm results in doxorubicin-induced cytotoxicity in folate receptor (FAR)-positive KB cancer cells as potent as UV irradiation (Figure 3C), whereas it accounts for more effective H_2S release in a pork skin model due to its deep tissue irradiation than UV (Figure 3D). This NIR control is equally demonstrated in a range of payloads from doxorubicin [9,14,90] to macromolecular

CRISPR-Cas9 [104]. Further benefits conferred by UCN relate to irradiation at NIR, which shows deeper tissue penetration compared to UV or visible light. Additionally, its luminescent bands contribute to UCN imaging and tracking as well [14,60,104,115].

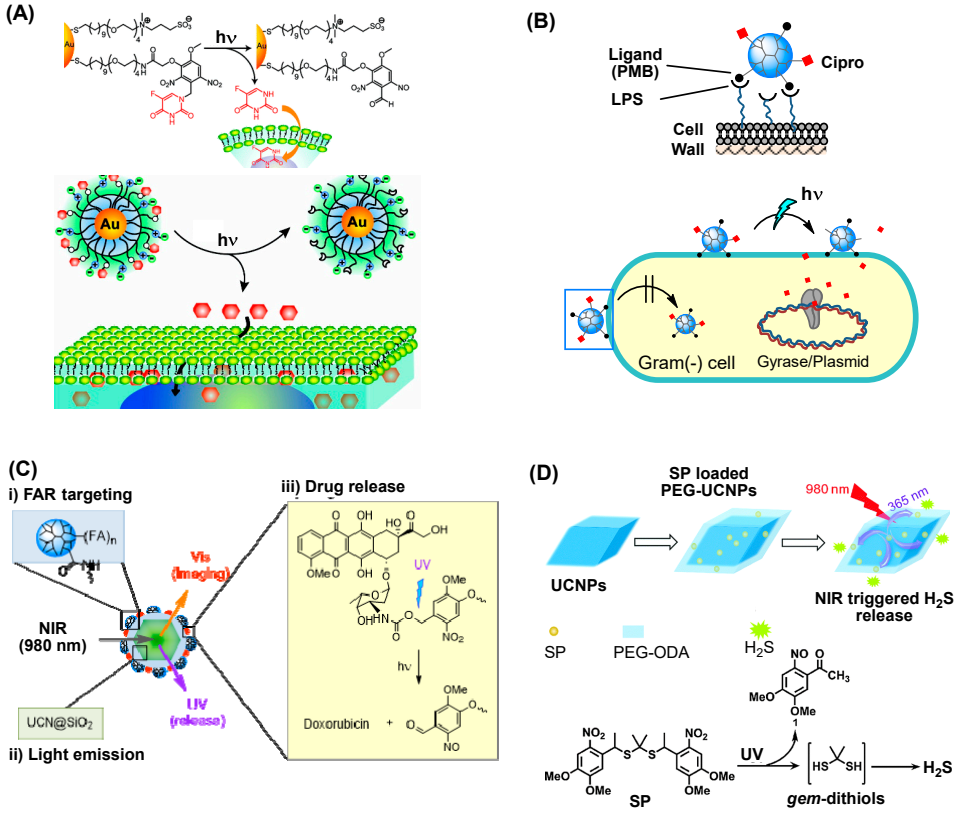

Figure 3. Representative strategies of therapeutic release via linker photolysis. (**A**) UV controlled release of 5-fluorouracil (5-FU)@AuNP [81]. Reproduced with permission, Copyright 2009, American Chemical Society. (**B**) Light-controlled delivery of ciprofloxacin at Gram (−) cells using lipopolysaccharide (LPS)-targeting dendrimer [10]. Reproduced with permission, Copyright 2016, Royal Society of Chemistry. (**C**) Near IR (NIR)-controlled doxorubicin release from folate receptor (FAR)-targeting upconversion nanocrystal (UCN) via linker photolysis by luminescence emission from UCN [14]. Reproduced with permission, Copyright 2015, John Wiley & Sons. (**D**) NIR-controlled H_2S release from its precursor and UCN-loaded nanogel [111]. Reproduced with permission, Copyright 2015, Royal Society of Chemistry.

In brief, release strategies via linker photolysis have yielded a remarkable growth in delivery systems. They have shown broad utilities in a variety of nanoscale systems including polymer [83,87,106], polymer micelle [87,94,97,116], PAMAM dendrimer [9–11,91,92,100], UCN [14,90,98,103–105,110] ($LiNbO_3$ [84]), AuNP [81,101], silver nanoparticle (AgNP) [102], quantum dot (QD) [89,107], TiO_2 [109], $mSiO_2$ [95], graphene [108], RNA nanocage [93], and hydrogel [99].

3.2. Disassembly

Release systems via disassembly are designed in diverse ways though their mechanisms occur mainly through linker photolysis [51,59,117–125] or photoisomerization. Systems that are applicable for photolytic disassembly rely on photodegradable soft nanomaterials made of liposome [117,118], polymer [125], polymer micelle [119–121,123,124,126,127], polymersome [51], tubisome [122], and functionalized UCN [59–61]. These are applicable for loading various therapeutic agents that include doxorubicin [51,59,121–123,126,127], camptothecin [125], siRNA [61], and aptamer Sgc8 [124]. Co-loading a fluorescent dye (6-carboxyfluorescein [117], Nile red [119,120]) or an MRI

contrast agent [118] serves as a route for monitoring drug release under image guidance. This is highlighted in Figure 4 with photocleavable liposomes loaded with Gd chelates demonstrated for MRI-guided delivery (Figure 4A) [118]. Upon irradiation at 400 nm, this liposome shows a time-dependent decrease in relaxivity (mM^{-1} s^{-1}) in a consistent manner with a decrease in its ONB absorbance at 365 nm.

Disassembly via photoisomerization occurs in systems incorporated with light-responsive units that undergo bond isomerization including azobenzene [128] or donor–acceptor Stenhouse adduct [129]. These units are readily incorporated in a range of nanomaterials from liposomes [128], polymer micelles [129–134], hydrogel [135,136], and metal-organic frameworks [137], to UCN [138]. These disassembly systems are successfully applied in the delivery of various payloads including erlotinib [130], 5-fluorouracil [137], doxorubicin [134], ciprofloxacin [136], propranolol [131], siRNA [132], and green fluorescent protein [135].

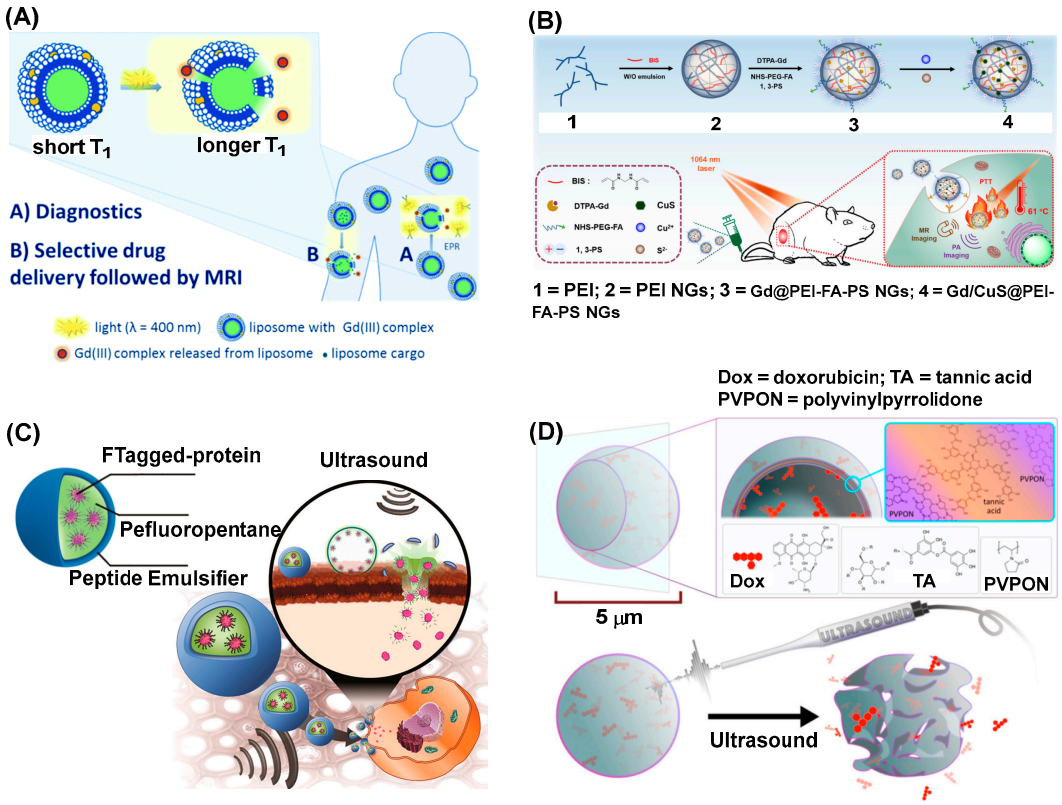

Figure 4. Representative strategies of therapeutic release via controlled disassembly. (**A**) Light-activated liposome disassembly for magnetic resonance imaging (MRI) contrast imaging and therapeutic release [118]. Reproduced with permission, Copyright 2019, Royal Society of Chemistry. (**B**) MRI and photoacoustic image-guided photothermal ablation therapy using a polyethylenimine (PEI)-based nanogel carrying Gd/CuS@PEI-FA-PS [139]. Reproduced with permission, Copyright 2020, American Chemical Society. (**C**) Ultrasound (US)-triggered cytosolic delivery of green fluorescent protein (GFP) loaded in fluorous nanoemulsions [140]. Reproduced with permission, Copyright 2020, American Chemical Society. (**D**) US triggered release of encapsulated doxorubicin (Dox) from polymer microcapsules via capsule perforation and destruction [141]. Reproduced with permission, Copyright 2017, American Chemical Society.

3.3. Gating

Gating refers to a process in which a payload is retained in a carrier until it is released upon gate opening. One approach involves a mechanism that induces photolytic alteration at a gate entrance by which its gate is opened (Figure 5). As shown in Figure 5A, this often occurs in porous materials

like mesoporous silica nanoparticle (MSN), which is temporarily blocked at its gate entrance with a photocleavable valve [69,142,143] or polymer brush [68,115,144]. This system is effective for NIR (974 nm)-controlled doxorubicin delivery in HeLa cells as evidenced with the induction of potent cytotoxicity [69]. Another approach involves valve isomerization at the entrance as illustrated in Figure 5B [143]. Its delivery application is consistent with UV-controlled release of doxorubicin which results in the induction of cytotoxicity in macrophages. Molecular valves commonly utilized in this isomerization approach comprise azobenzne [71,143,145,146], coumarate [147], fumaramide [148], spiropyran [149], and donor–acceptor Stenhouse adduct [150]. Their role in gated release is well established by applications in various payloads including doxorubicin [71,143,145,146,150], camptothecin [150], naproxen [147], curcumin [151], DNA [152], and dye molecules including rhodamine B [148] and 4′,6-diamidino-2-phenylindole [149].

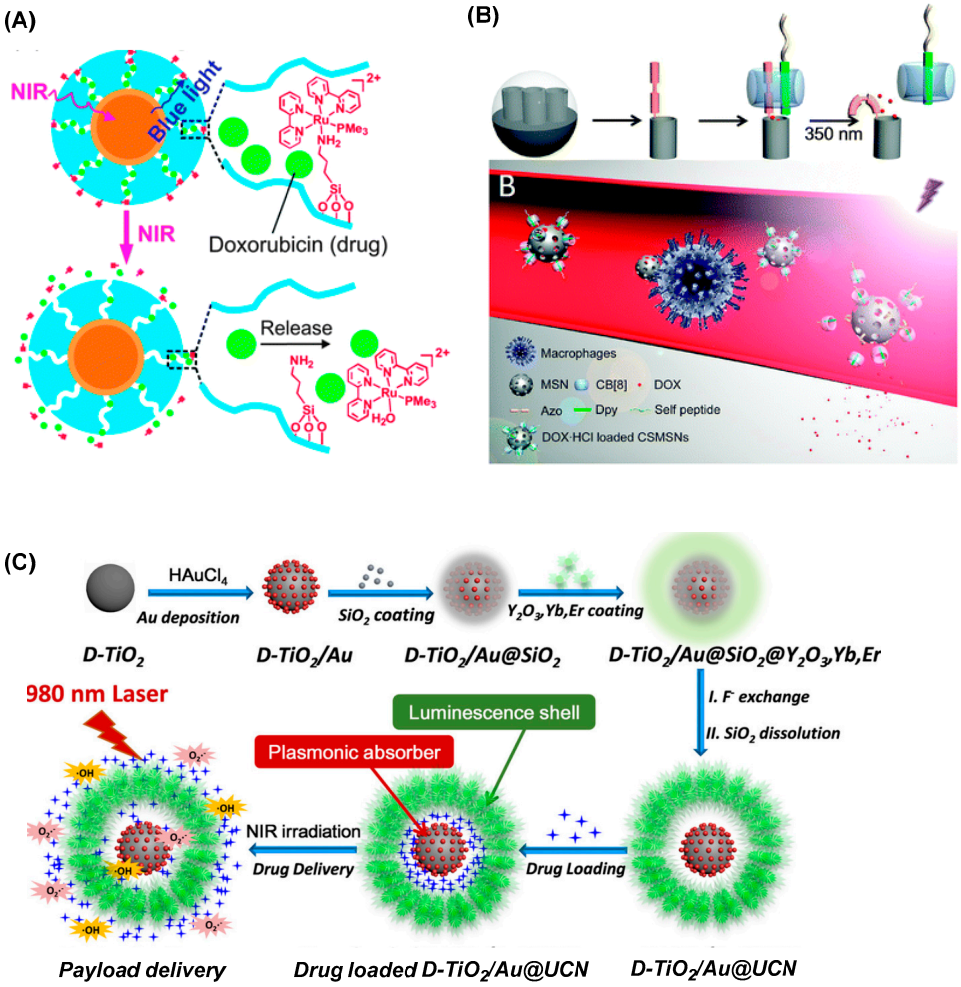

Figure 5. Representative strategies of therapeutic release via controlled gating. (**A**) Doxorubicin release via NIR-triggered cleavage of a Ru complex valve in $mSiO_2$-coated UCN [69]. Reproduced with permission, Copyright 2015, Royal Society of Chemistry. (**B**) Doxorubicin release via photoisomerization at a gate entrance in mesoporous silica nanoparticle (MSN) [143]. Reproduced with permission, Copyright 2015, Royal Society of Chemistry. (**C**) NIR light-controlled release of ampicillin from TiO_2/Au@UCN nanocomposite [153]. Reproduced with permission, Copyright 2020, American Chemical Society.

Whereas most gating systems are designed for activation by UV or visible light, they can be functionalized for opening by NIR. This is achieved by integration of valve-attached $mSiO_2$ with nano gold [68] or UCN [153], each serving as an NIR-responsive nanomaterial. Of note is a TiO_2/Au@UCN

nanocomposite (Figure 5C), a dual action system designed for NIR-controlled ampicillin release and ROS production by irradiation at 980 nm. This shows potent antibacterial activities against *E. coli* and methicillin-resistant *Staphylococcus aureus* (MRSA) in vitro [153]. Their gate opening occurs through valve alteration or isomerization in response to photothermal heating by nano Au or UV–VIS luminescence emitted from NIR-excited UCN. This NIR control has been successfully applied to several payloads including doxorubicin [68,69,143], fluorescein [115,144], and ruthenium-bipyridyl [142].

Briefly, light control constitutes one of principal strategies employed in the activation of nanotherapeutic systems. Its mechanisms for therapeutic release occur via linker photolysis, disassembly, or pore gating.

4. Photodynamic Activation

4.1. Reactive Oxygen Species (ROS)

Photodynamic activation involves the production of reactive oxygen species (ROS) which comprise singlet oxygen ($^1O_2$) and oxygen-based radical species [154,155]. This occurs through photosensitizer (PS) excitation as applicable to zinc phthalocyanine (ZnPc) [156,157], chlorin e6 (Ce6) [158], rose bengal [12,13], and NIR-responsive indocyanine dye [159]. Alternatively, ROS are produced by other types of PS based on photoactive polymers including polydopamine (Figure 2B) [47] and photoactive nanomaterials [76,160] including nanoTiO_2 [161]. ROS production by most PS systems occurs by light absorption at visible wavelengths. However, UCN-integrated PS systems [12,13,153,157,162,163] are able to produce ROS by NIR irradiation at 980 nm due to UCN luminescence at UV–VIS bands. This NIR-based PS activation is more beneficial in therapeutic applications in vivo than in vitro due to its deeper penetration [12,163].

4.2. Photodynamic Delivery Systems

A typical system designed for photodynamic delivery consists of PS molecules encapsulated or conjugated in nanomaterials like mesoporous nanoparticles (NPs) [156], liposomes [164–166], polymers [47,167,168], polymer micelles [65,67,159,169,170], and lipid NPs [171]. Due to high chemical reactivity, ROS produced from these systems are able to make a broad range of non-selective cellular damages from lipid oxidation responsible for membrane ruptures to oxidative degradation in proteins and nucleic acids [76,160]. This accounts for its potent cytotoxicity induced in mammalian cells and bacterial pathogens [154,172], and it serves as a therapeutic basis for photodynamic therapy (PDT) [155,173–175].

Moreover, ROS contributes to controlled drug release through its participation in oxidative linker cleavage, disassembly or gating [66]. This is illustrated with Ce6-bound IgG nanocomplexes, an anticancer system demonstrated for its ability to deliver an immune checkpoint inhibitor under fluorescent image guidance [176]. Photodynamic release is equivalently applied to a broad range of therapeutic agents from anticancer drugs including doxorubicin [65,66,167], paclitaxel [166], bortezomib [47], SN38 [67], camptothecin [159], mitoxantrone [169], and 7-dehydrocholesterol [165] to antibacterial agents vancomycin [168] and ampicillin [153]. UCN integration allows NIR-controlled photodynamic drug release as illustrated in Figure 5C where ampicillin is released from a UCN-coated TiO_2/Au nanocomposite [153].

In short, photodynamic activation serves as an important route for a dual therapy due to ROS-mediated cytotoxicity and the ability to participate in controlled drug release. PS systems also offer an optical imaging capability due to their fluorescence emission from PS or photoactive nanomaterials themselves, as frequently applied in image-guided delivery [170,174,177]. Their fluorescence detection is coupled with other imaging modes. This is illustrated with a Ce6-based system co-loaded with an Mn^{2+} chelate, which is designed for photodynamic therapy under dual image guidance by fluorescence and MRI [170,174,177].

4.3. Challenges in Photodynamic Systems

PS systems are faced with certain challenges that are attributable to unfavorable physicochemical properties and cellular occurrence of ROS resistance. Most PS molecules show poor aqueous solubility and high aggregation tendency because of their hydrophobic aromatic rings that engage in intermolecular π–π stacking interaction. As a consequence, these are responsible for lowered efficiency in ROS production, fluorescence quenching, or suboptimal imaging resolution. This issue can be overcome in part by ROS production using either photoactive nanomaterials or polymer particulates that display aggregation induced emission (AIE) [178,179], including integrin-targeting polymer nanodots [179].

Another challenge relates to occurrence of cellular ROS resistance, a known mechanism responsible for reduction in PDT efficacy. This occurs through reductive inactivation of ROS by intracellular antioxidant thiols, primarily, GSH. A few approaches are reported to address this problem including co-delivery of an Mn^{2+} contrast agent [177] or MnO_2, which releases thiol-oxidizing manganese ions [170]. Their oxidative role contributes to a decrease in GSH level via thiol oxidation. An alternative approach involves facilitating the rate of ROS production by increasing the intracellular concentration of O_2, a precursor molecule for ROS. This involves co-delivery of catalase, an oxidative enzyme that engages in catalyzing endogenous hydrogen peroxide to O_2 [170,180]. The latter approach is of most relevance to applications in tumors where their oxygen level remains relatively lower (hypoxia) than normal tissues. Potent antitumor efficacy is achieved by catalase co-delivery systems made of Ce6-modified chitosan micelles [170] or indocyanine green-loaded albumin complexes [180].

In short, photodynamic activation produces ROS for application in photodynamic therapy [155,158] as well as dual therapy by engagement in controlled drug release [176]. Photodynamic systems are applied for image-guided delivery through their fluorescence alone or in combination with MRI [170,177], photoacoustic imaging (PAI) [180], and/or thermal imaging [170].

5. Photothermal Activation

Certain classes of nanomaterials are able to produce localized heat through plasmonic photoactivation [181]. These comprise nano Au (AuNP, gold nanorod (AuNR) [182], hollow Au nanosphere (AuNS) [183]), black phosphorus [36], CuS [184], and MoS_2 nanosheet [185]. Their heat production results in the induction of cytotoxic hyperthermia, and this constitutes a therapeutic basis in photothermal ablation therapy (PTT) [186,187]. The heat is further exploited in release mechanisms for dual therapy. Additionally, it serves as an imaging modality applicable in photothermal imaging, which is widely applied in image-guided systems.

5.1. Photothermal Drug Release

Despite its cytotoxicity, it is possible that hyperthermia alone is not potent enough for complete tumor ablation, leaving a marginal area of tumor for potential recurrence. This insufficiency is improved by combination with drug release. Delivery systems ideal for photothermal release are designed through nanomaterial integration that consists of a drug-loadable porous nanomaterial and, separately, a photothermally-active nanomaterial. Their integration is illustrated with various combinations of nano Au and $mSiO_2$ including smaller AuNR-loaded $mSiO_2$ [188], Au-coated $mSiO_2$ [74], $mSiO_2$-coated AuNR [72], and UCN coated with carbon dot-loaded $mSiO_2$ [73].

Photothermal drug release occurs through one of two main mechanisms, pore opening and disassembly. First, pore opening occurs in a system when a local temperature is elevated by photothermal activation. This photothermal release is applied to doxorubicin [72,73], naproxen [188], and ibuprofen [74] loaded in porous silica oxide. Second, disassembly occurs in thermally unstable nanomaterials including liposomes co-loaded with nano Au [189] or black phosphorous QD [190]. Polymer micelles are equivalently applied for photothermal disassembly as illustrated with those encapsulated with nano Au (AuNR [63,191,192], Au nanoflower [193]), polydopamine [194],

or photothermal dyes including cypate [195], indocyanine green [196,197], and BODIPY [64]. Other systems designed for the photothermal disassembly include drug-loaded Au nanoshell [198] and nano Au-coated polymer particulates [199]. Overall, nanomaterials integrated for photothermal activation are successfully applied to a variety of payloads from doxorubicin [62,190,192,196], camptothecin [64], berberine [189], cisplatin [200], Pt (IV) prodrug [195,197], plasmid DNA [191,199], and siRNA [199] to precursor DNAzyme [198].

5.2. Photothermal Imaging Delivery

Heat production itself serves as an imaging modality in photothermal systems. This is illustrated with AuNR-coated $mSiO_2$ developed for photothermal image-guided dual therapy via hyperthermia and 5-fluorouracil release [182]. A few other systems have been developed similarly that include UCN (Gd_2O_3:Yb,Er)-coated nano Au [201], black phosphorus-loaded hydrogel [36], polydopamine-coated IONP [202], or extracellular vesicles loaded with Au–IONP [203]. Each of these is effectively applied in the photothermal delivery of doxorubicin [36] or anti-miR-21 aptamer [203] under imaging guidance. Yet, unlike purely imaging modalities, such as MRI scans, photothermal imaging has a risk of inducing premature cytotoxicity or drug activation by photothermal heat produced during its scanning process. Therefore, its application is limited on photothermal verification or optimization purposes at target tissues instead of pre-activation imaging guidance, which is achieved by supplementary modalities such as MRI [201], fluorescence [36,182], and PAI [182,202].

5.3. Photoacoustic Imaging (PAI) Delivery

The technique of PAI is based on detecting a sound wave (photoacoustic signal) which is generated upon photoexcitation at certain functional systems. It occurs via photothermal expansion (thermoelastic), vaporization (perfluoro molecule), and nanomaterial breakdown [37]. Photoacoustic systems are designed with chromophore molecules or photoactive nanomaterials including polydopamine [202], AuNR [204], CuS [139], and MoS_2 [205]. These are integrated in various ways by nanomaterial coating [202], encapsulation in nanobubbles [204], or loading in a nanogel [139]. These include a paclitaxel-loaded multifunctional nanobubble composed of AuNR and perfluorohexane [204]. Its photoacoustic activation involves perfluorohexane vaporization that occurs in response to temperature elevation induced by photoactivated AuNR. This leads to shockwave production that triggers bubble implosion, serving as a mechanism for drug release and PAI [204]. Systems loaded with CuS [139] and MoS_2 [205] are reported as well for PAI-guided photothermal therapy as illustrated with a FAR-targeted polyethylenimine (PEI)-based nanogel loaded with CuS and Gd chelates (Figure 4B) [139]. This nanogel system allows dual image (PAI, MRI)-guided PTT in FAR-overexpressing tumors by laser irradiation at 1064 nm. In a similar way, MoS_2 nanosheet modified with IONP and ^{64}Cu on its shell surface shows a multifunctional capability that allows PAI-guided PTT in combination with two complementary imaging modes, MRI and PET [205].

5.4. Computed Tomography (CT) Imaging Delivery

CT-guided photothermal systems rely on nanomaterials with ability for X-ray absorption. These comprise nano Au [206], CuS [184], CuS-Pt [207], Bi_2Se_3 nanosponge [208], and MoS_2 nanosheet [185], and many of these exhibit strong absorbance at NIR wavelengths. Therefore, CT systems allow additional imaging capabilities including thermal imaging and PAI [208]. Examples of CT-guided delivery include doxorubicin-loaded MoS_2 nanosheet [185] and CuS-encapsulated hyaluronic acid polymer [184]. Liposomes loaded with IONP@Au are effectively applicable for dual CT and magnetic particle imaging as demonstrated in the delivery of tenofovir disoproxil, an antiviral drug, in HIV-infected microglia cells [206]. Using Bimetallic CuS-Pt is dually beneficial for CT guidance as well as Pt chemotherapy in which cytotoxic Pt (II) is released inside the cell following its photothermal activation at 808 nm [207].

5.5. Positron Emission Tomography (PET) Imaging Delivery

The basis of PET imaging relies on detecting γ-rays generated in a tissue when tissue electrons react with positrons emitted from radionucleotide tracers carried in a delivery system [209]. PET tracers used in clinical agents include ^{11}C, ^{13}N, ^{15}O, and ^{18}F, each incorporated as an isotope in a ligand or drug molecule. Post-transition metal elements constitute another class of PET tracers that includes ^{89}Zr [45], ^{64}Cu [205,210,211], and Au [212]. PET systems developed for drug delivery are designed in a number of ways. First, PET tracers are incorporated as a part of the carrier as illustrated with ^{89}Zr incorporated in a metal-organic framework [45], a system developed for doxorubicin delivery under PET guidance. Second, some of these tracers are available as chelated species as seen in ^{64}Cu chelated in polymer micelles [211] and ^{64}Cu-NOTA conjugated to $mSiO_2$ [213]. Third, PET tracers allow direct integration through chemoadsorption or coating as evident in ^{64}Cu-adsorbed MoS_2 nanosheets [205], Au-coated PdCu nanotripods [212], and ^{64}Cu-coated AuNR [210]. Overall, CT imaging systems designed in these ways are applied for therapeutic delivery. This includes doxorubicin-loaded $mSiO_2$@^{64}Cu-NOTA demonstrated for tumor vasculature-targeted delivery under PET imaging [213]. Nanodots composed of ^{64}CuS display a similar capability for PET-guided photothermal ablation as demonstrated in tumor-bearing mice [214].

5.6. Single Photon-Emission Computerized Tomography (SPECT) Imaging Delivery

SPECT is a dual imaging modality composed of CT and radiation imaging [209]. Like PET, radionuclide elements are required that include ^{111}In, ^{123}I, ^{131}I, ^{99m}Tc, and ^{188}Re, and they are often incorporated in aromatic compounds through $^{123}I/^{131}I$ labeling [139] and in pharmaceuticals through ^{99m}Tc-chelation [209]. Radionucleotide tracers used in SPECT have longer half-lives (6–68 h) on average than PET tracers. This property is highly beneficial during their radiolabeling, nanomaterial incorporation, and uses because it allows more time until full decay.

Several systems have been reported for SPECT-guided therapy based on nano Au [183], dendrimer [139], and liposomes [215]. These include ^{111}In-labeled hollow AuNS designed for epidermal growth factor receptor (EGFR)-targeted photothermal ablation in head and neck cancer [183]. ^{131}I-labeled dendrimer is effectively used as a tumor-targeted radionuclide therapy after ligand functionalization with a tumor targeting the LyP-1 peptide [139]. Micelle serves as another platform for SPECT-guided delivery as illustrated with ^{188}Re-labeled micelles loaded with IR-780 dye applied for PTT in tumors [215].

6. Ultrasound Activation

6.1. Mechanism of Ultrasound Activation

Low-intensity ultrasound (US) is commonly used in diagnostic ultrasonography [38], however high-intensity US can serve as an external stimulus strong enough for inducing therapeutic release. This US activation occurs in nanomaterial systems composed of gas-filled cavities or US-responsive molecules including perfluorocarbon [140,216], fluorous tag [20], and polymer [141]. Like photoacoustic activation described above, the physical basis of US activation involves cavitation which occurs upon vaporization of molecules loaded in the cavity. This leads to induction of bubble ruptures or open pores, both contributing to drug release as illustrated in Figure 4C,D [20]. This is evident in A549 cells treated with GFP-loaded fluorous nanoemulsions that show a significant increase in intracellular fluorescence following US application compared to free GFP as a control (Figure 4C). Similarly, stimulating microcapsule-treated MCF-7 cells by therapeutic US leads to induction of cytotoxicity, which does not occur without microcapsule treatment or by diagnostic weaker US (Figure 4D).

High-intensity focused ultrasound (HIFU) is also able to induce hyperthermia, which serves as another mechanism applicable for controlled drug release [22]. Similar to photothermal activation, this occurs in thermo-sensitive systems [22] including doxorubicin-loaded liposomes, which show

controlled drug release in response to high-intensity US [217,218]. In spite of its potential and recent advances in transducer designs, the efficacy of HIFU activation is limited by its focal length that can reduce spatial resolution, its slow onset of activation which takes hours, and its challenges in certain tissue areas that require crossing a bone or intact skull [219].

6.2. Ultrasound Delivery Systems

Delivery systems that are responsive to US activation comprise microbubbles [20,21,220], nanobubbles [216], probubbles [221], nanoemulsions [140], nanodroplets [222], and microcapsules [141]. Microbubbles are popularly used in US applications due to their large shell or cavity space available for loading supplementary imaging probes and therapeutic agents. These include IONP (Fe_3O_4)-coated microbubbles developed for dual MRI and US-guided delivery of tPA [21]. Multifunctional nanobubbles that are loaded with 5-fluorouracil, a Gd chelate and IR-780 dye, are comparably used in US-controlled drug release under guidance by multiple imaging modalities [216]. US activation is also applied in the controlled release of gas molecules as illustrated with liposomal probubbles loaded with a H_2S precursor for application in tumor ablation therapy [221]. Non-bubble US systems are made of nanoemulsions (Figure 4C) [140], microcapsules (Figure 4D) [141], and nanodroplets [222], each applied in the delivery of doxorubicin [141], green fluorescent protein and antibodies [140], and paclitaxel [222], respectively. Porous nanomaterials are useful as well for US activation. This is illustrated with $mSiO_2$ loaded with an NO precursor and superparamagnetic iron oxide nanoparticle (SPION) for MRI-guided, US-controlled NO release in tumor [223].

One of the limitations in US systems relates to bubble sizes. Most microbubble systems are excellent in contrast imaging capability, although they are considerably too large for efficient tissue penetration and cellular uptake. On the other hand, nanometer-sized systems are reversed in the trend with greater tissue infiltration at lower imaging contrast. This conflicting unbalance has been recently addressed using size-variable polymersome (~200 nm), which is able to grow in size under acidic conditions [224]. Thus, once taken up in tumor tissues and subcellular compartments, its signal intensity in US imaging is enhanced as a result of its enlarged size.

In summary, US has been actively explored for therapeutic activation in image-guided delivery systems. This strategy is applied to a variety of payloads from drugs (doxorubicin [141,224], paclitaxel [20,222]) and proteins (tissue plasminogen activators [21], green fluorescent protein [140], antibodies [140]) to gas molecules of therapeutic significance (H_2S [221], NO [223]).

7. Electric and Magnetic Field Activation

Stimulation under an electrical field is potentially applicable in controlled delivery systems. A notable approach involves electroporation, a technique that applies an electrical pulse to induce temporary pores across cell membranes. This technique has played an important role in enhancing cell permeability as often applied to small drug molecules, biomolecules, and genes [225,226]. However, it is rarely used in nanomaterial delivery though it can be beneficial as illustrated with doxorubicin-loaded SPION demonstrated for tumor uptake through electroporation [227]. Unlike normal electroporation, this system offers an imaging guidance through magnetic particle imaging that helps precise positioning of electrodes at its uptake area.

Applying an alternating magnetic field (AMF) on magnetic nanomaterials is more often used in delivery systems. It is able to produce a localized heat applicable for controlled drug release [3]. This magnetic hyperthermia is observed in IONP systems loaded with DNA [228] or doxorubicin linked through a thermally unstable azo bond [229]. SPION is equally applicable for magnetically induced hyperthermia demonstrated in photothermal therapy [230]. Its use also plays a critical role in MPI-guided spatial and temporal control of magnetic hyperthermia, drug delivery, or the combination of these [230–232]. This approach helps to attain precise localization and positioning of magnetic nanocarriers within a target region prior to drug release through AMF-triggered hyperthermia. This is demonstrated with SPION-encapsulated poly(lactic-co-glycolic acid) (PLGA) [232] and

doxorubicin-loaded liposomes [231]. Furthermore, applying a magnetic field serves as a physical force that enables the control of particle movement. Therefore, drug-loaded magnetic nanomaterials are guided and transported by a magnet for accumulation in a targeted tissue, which has been effectively applied in a few systems. These include a magnetic nanospear designed for gene transfection in glioblastoma cells [233], SPION-loaded microbubbles for doxorubicin delivery in brain tumors [217], and IONP-coated microbubbles for accumulation at specific blood vessels [21]. Overall, delivery systems developed for magnetic control offer several benefits including magnetically inducible hyperthermia, magnetic particle imaging, and magnetic particle guidance.

8. Conclusions and Perspectives

This article described recent advances in nanotherapeutic systems developed for image-guided delivery with a focus on their design concepts and mechanisms in therapeutic activation. Some of their mechanisms are attributed to cellular and pathophysiological factors, primarily low pH conditions [35,45,46] or elevated GSH levels [49]. Other mechanisms involve external stimulations which are more actively controlled via light-triggered linker cleavage [11,81,91,92,101], disassembly [59–67], pore gating [68–74], photothermal activation [36,182,204], photodynamic activation [156,164–166], US-mediated disassembly [140,141,216], hyperthermia [217], electroporation [227], and magnetic thermal activation [230]. Developing these activation strategies is making a significant impact on advancing knowledge and creating a new capability in nanotherapeutic delivery systems.

It is however worth noting current limitations associated with activation strategies. The degree of spatial resolution conferred by each activation strategy is variable as it is defined by the perimeter of its stimulus. Some strategies characterized by US, electromagnetic field, or thermal stimulation show relatively lower precision in spatiotemporal control compared to light activation. On the other hand, light shows a lower level of tissue penetration compared to US or electromagnetic stimulation [80]. This light limitation is currently worked out using an optical technique that allows tissue bypassing in which laser irradiation is delivered through a catheter inserted in a needle injected in tissue [201].

Another critical aspect which is of broad interest involves how to achieve specific nanomaterial uptake and localization in targeted cells only. Many systems discussed here are designed for tumor uptake via enhanced permeation and retention (EPR), a passive targeting strategy that facilitates particle infiltration through leaky vessels in tumors (Figure 1) [234]. However, this passive targeting is not applicable for distinguishing specific tumor biomarkers or targeted binding and uptake at specific biomarker-overexpressing tumor cells. This lack of specificity is achieved otherwise by an active targeting strategy [3,235,236] in which a drug-loaded nanomaterial is functionalized through multivalent conjugation with a target-specific ligand or antibody. This active targeting has been applied to a few tumor biomarkers that include FAR [46,204,216], $\alpha_v\beta_3$ integrin [179,210,237,238], IGF1 receptor [48], EGFR [183], CD105 [213], CCR5 [212], and nucloelin [45]. It would be equally applicable to other promising but less explored biomarkers that include prostate-specific membrane antigen (PSMA) receptors [239], Her2 [240], riboflavin receptors [241,242], and transferrin receptors [243] for brain delivery. In brief, multivalent ligand conjugation serves as an important strategy in the design of actively targeted systems.

Finally, clinical translation of nanotherapeutic agents is associated with significant challenges due to their multifunctional design, difficulty in synthetic scalability, and paucity of efficient clinical devices needed for their optimal activation. Nevertheless, they show a growing potential as evident with numerous types of nanotherapeutic agents either approved or advanced to clinical studies [244]. Of those, release control by endogenous factors is most actively engaged as shown in PLGA NPs encapsulated with leuprolide (Eligard®) [245], albumin NPs bound with paclitaxel (Abraxane®) [246], and liposomes encapsulated with doxorubicin (Doxil®) [247], mifamurtide (Mepact®) [248], vincristine (Marqibo®) [249], or irinotecan (Onivyde®) [250]. Thermal control of drug release is also successfully applied in heat-sensitive liposomes loaded with doxorubicin (ThermoDox®) [251]. Clinical development of photoactivated nanotherapeutics has been relatively

slower but was already demonstrated by PDT-based verteporfin liposome (Visudyne®), which is approved for age-related macular degeneration and is currently being investigated for locally advanced pancreatic cancer [252,253]. This strategy is also applicable in topical and superficial treatments as illustrated with PDT nanoemulsion (BF-200) [254], a topical agent investigated for treating actinic keratosis [255]. In summary, nanotherapeutic activation strategies are currently being evaluated for their clinical translation [39,244].

Funding: This research received no external funding.

Acknowledgments: The author acknowledges support for cited works in part by the Michigan Nanotechnology Institute for Medicine and Biological Sciences.

Conflicts of Interest: The author declares no competing financial interests.

References

1. Ojha, T.; Rizzo, L.; Storm, G.; Kiessling, F.; Lammers, T. Image-guided drug delivery: Preclinical applications and clinical translation. *Expert Opin. Drug Deliv.* **2015**, *12*, 1203–1207. [CrossRef] [PubMed]
2. Choi, S.K. (Ed.) Photocleavable linkers: Design and applications in nanotechnology. In *Photonanotechnology for Therapeutics and Imaging*; Elsevier: Amsterdam, The Netherlands, 2020; pp. 243–275.
3. Wong, P.T.; Choi, S.K. Mechanisms of Drug Release in Nanotherapeutic Delivery Systems. *Chem. Rev.* **2015**, *115*, 3388–3432. [CrossRef] [PubMed]
4. Wang, Y.; Kohane, D.S. External triggering and triggered targeting strategies for drug delivery. *Nat. Rev. Mater.* **2017**, *2*, 17020. [CrossRef]
5. Zhang, Y.; Xu, C.; Yang, X.; Pu, K. Photoactivatable Protherapeutic Nanomedicine for Cancer. *Adv. Mater.* **2020**, *32*, 2002661. [CrossRef]
6. Tiwari, P.M.; Vig, K.; Dennis, V.A.; Singh, S.R. Functionalized Gold Nanoparticles and Their Biomedical Applications. *Nanomaterials* **2011**, *1*, 31–63. [CrossRef]
7. Yin, R.; Agrawal, T.; Khan, U.; Gupta, G.K.; Rai, V.; Huang, Y.-Y.; Hamblin, M.R. Antimicrobial photodynamic inactivation in nanomedicine: Small light strides against bad bugs. *Nanomedicine* **2015**, *10*, 2379–2404. [CrossRef]
8. Zhao, J.; Duan, L.; Wang, A.; Fei, J.; Li, J. Insight into the efficiency of oxygen introduced photodynamic therapy (PDT) and deep PDT against cancers with various assembled nanocarriers. *WIREs Nanomed. Nanobiotechnol.* **2020**, *12*, e1583. [CrossRef]
9. Wong, P.T.; Tang, S.; Cannon, J.; Chen, D.; Sun, R.; Lee, J.; Phan, J.; Tao, K.; Sun, K.; Chen, B.; et al. Photocontrolled Release of Doxorubicin Conjugated through a Thioacetal Photocage in Folate-Targeted Nanodelivery Systems. *Bioconjug. Chem.* **2017**, *28*, 3016–3028. [CrossRef]
10. Wong, P.; Tang, S.; Mukherjee, J.; Tang, K.; Gam, K.; Isham, D.; Murat, C.; Sun, R.; Baker, J.R.; Choi, S.K. Light-Controlled Active Release of Photocaged Ciprofloxacin for Lipopolysaccharide-Targeted Drug Delivery using Dendrimer Conjugates. *Chem. Commun.* **2016**, *52*, 10357–10360. [CrossRef]
11. Choi, S.K.; Thomas, T.; Li, M.; Kotlyar, A.; Desai, A.; Baker, J.R., Jr. Light-Controlled Release of Caged Doxorubicin from Folate Receptor-Targeting PAMAM Dendrimer Nanoconjugate. *Chem. Commun.* **2010**, *46*, 2632–2634. [CrossRef]
12. Xu, F.; Zhao, Y.; Hu, M.; Zhang, P.; Kong, N.; Liu, R.; Liu, C.; Choi, S.K. Lanthanide-doped core-shell nanoparticles as a multimodality platform for imaging and photodynamic therapy. *Chem. Commun.* **2018**, *54*, 9525–9528. [CrossRef] [PubMed]
13. Xu, F.; Hu, M.; Liu, C.; Choi, S.K. Yolk-structured multifunctional up-conversion nanoparticles for synergistic photodynamic-sonodynamic antibacterial resistance therapy. *Biomater. Sci.* **2017**, *5*, 678–685. [CrossRef] [PubMed]
14. Wong, P.T.; Chen, D.; Tang, S.; Yanik, S.; Payne, M.; Mukherjee, J.; Coulter, A.; Tang, K.; Tao, K.; Sun, K.; et al. Modular Integration of Upconversion Nanocrystal-Dendrimer Composites for Folate Receptor-Specific Near Infrared Imaging and Light Triggered Drug Release. *Small* **2015**, *11*, 6078–6090. [CrossRef] [PubMed]
15. Cai, W.; Wang, J.; Chu, C.; Chen, W.; Wu, C.; Liu, G. Metal–Organic Framework-Based Stimuli-Responsive Systems for Drug Delivery. *Adv. Sci.* **2019**, *6*, 1801526. [CrossRef] [PubMed]

16. Huang, J.; Li, Y.; Orza, A.; Lu, Q.; Guo, P.; Wang, L.; Yang, L.; Mao, H. Magnetic Nanoparticle Facilitated Drug Delivery for Cancer Therapy with Targeted and Image-Guided Approaches. *Adv. Funct. Mater.* **2016**, *26*, 3818–3836. [CrossRef]
17. Wang, J.; Li, N. Functional hollow nanostructures for imaging and phototherapy of tumors. *J. Mater. Chem. B* **2017**, *5*, 8430–8445. [CrossRef]
18. Gullotti, E.; Yeo, Y. Extracellularly Activated Nanocarriers: A New Paradigm of Tumor Targeted Drug Delivery. *Mol. Pharmaceutics* **2009**, *6*, 1041–1051. [CrossRef]
19. Chen, H.H.W.; Song, I.-S.; Hossain, A.; Choi, M.-K.; Yamane, Y.; Liang, Z.D.; Lu, J.; Wu, L.Y.-H.; Siddik, Z.H.; Klomp, L.W.J.; et al. Elevated Glutathione Levels Confer Cellular Sensitization to Cisplatin Toxicity by Up-Regulation of Copper Transporter hCtr1. *Mol. Pharmacol.* **2008**, *74*, 697–704. [CrossRef]
20. Zhu, X.; Guo, J.; He, C.; Geng, H.; Yu, G.; Li, J.; Zheng, H.; Ji, X.; Yan, F. Ultrasound triggered image-guided drug delivery to inhibit vascular reconstruction via paclitaxel-loaded microbubbles. *Sci. Rep.* **2016**, *6*, 21683. [CrossRef]
21. Wang, S.; Guo, X.; Xiu, W.; Liu, Y.; Ren, L.; Xiao, H.; Yang, F.; Gao, Y.; Xu, C.; Wang, L. Accelerating thrombolysis using a precision and clot-penetrating drug delivery strategy by nanoparticle-shelled microbubbles. *Sci. Adv.* **2020**, *6*, eaaz8204. [CrossRef]
22. Grüll, H.; Langereis, S. Hyperthermia-triggered drug delivery from temperature-sensitive liposomes using MRI-guided high intensity focused ultrasound. *J. Control. Release* **2012**, *161*, 317–327. [CrossRef]
23. Li, F.; Qin, Y.; Lee, J.; Liao, H.; Wang, N.; Davis, T.P.; Qiao, R.; Ling, D. Stimuli-responsive nano-assemblies for remotely controlled drug delivery. *J. Control. Release* **2020**, *322*, 566–592. [CrossRef]
24. Hatefi, A.; Minko, T. Advances in image-guided drug delivery. *Drug Deliv. Transl. Res.* **2012**, *2*, 1–2. [CrossRef]
25. Solorio, L.; Patel, R.B.; Wu, H.; Krupka, T.; Exner, A.A. Advances in image-guided intratumoral drug delivery techniques. *Ther. Deliv.* **2010**, *1*, 307–322. [CrossRef]
26. Chakravarty, R.; Hong, H.; Cai, W. Positron Emission Tomography Image-Guided Drug Delivery: Current Status and Future Perspectives. *Mol. Pharm.* **2014**, *11*, 3777–3797. [CrossRef] [PubMed]
27. Tomitaka, A.; Arami, H.; Ahmadivand, A.; Pala, N.; McGoron, A.J.; Takemura, Y.; Febo, M.; Nair, M. Magneto-plasmonic nanostars for image-guided and NIR-triggered drug delivery. *Sci. Rep.* **2020**, *10*, 10115. [CrossRef] [PubMed]
28. Chung, C.; Brock, K. Image-guided radiation therapy: Looking beyond what we currently see. *Future Oncol.* **2017**, *13*, 2317–2319. [CrossRef] [PubMed]
29. Gao, D.; Guo, X.; Zhang, X.; Chen, S.; Wang, Y.; Chen, T.; Huang, G.; Gao, Y.; Tian, Z.; Yang, Z. Multifunctional phototheranostic nanomedicine for cancer imaging and treatment. *Mater. Today Bio* **2020**, *5*, 100035. [CrossRef]
30. Liong, M.; Lu, J.; Kovochich, M.; Xia, T.; Ruehm, S.G.; Nel, A.E.; Tamanoi, F.; Zink, J.I. Multifunctional Inorganic Nanoparticles for Imaging, Targeting, and Drug Delivery. *ACS Nano* **2008**, *2*, 889–896. [CrossRef]
31. Wojtynek, N.E.; Mohs, A.M. Image-guided tumor surgery: The emerging role of nanotechnology. *WIREs Nanomed. Nanobiotechnol.* **2020**, *12*, e1624. [CrossRef]
32. Pablico-Lansigan, M.H.; Situ, S.F.; Samia, A.C.S. Magnetic particle imaging: Advancements and perspectives for real-time in vivo monitoring and image-guided therapy. *Nanoscale* **2013**, *5*, 4040–4055. [CrossRef] [PubMed]
33. Wu, K.; Su, D.; Saha, R.; Liu, J.; Chugh, V.K.; Wang, J.-P. Magnetic Particle Spectroscopy: A Short Review of Applications Using Magnetic Nanoparticles. *ACS Appl. Nano Mater.* **2020**, *3*, 4972–4989. [CrossRef]
34. Jiang, S.; Gnanasammandhan, M.K.; Zhang, Y. Optical imaging-guided cancer therapy with fluorescent nanoparticles. *J. R. Soc. Interface* **2010**, *7*, 3–18. [CrossRef] [PubMed]
35. Zou, Y.; Li, D.; Wang, Y.; Ouyang, Z.; Peng, Y.; Tomás, H.; Xia, J.; Rodrigues, J.; Shen, M.; Shi, X. Polyethylenimine Nanogels Incorporated with Ultrasmall Iron Oxide Nanoparticles and Doxorubicin for MR Imaging-Guided Chemotherapy of Tumors. *Bioconjug. Chem.* **2020**, *31*, 907–915. [CrossRef]
36. Qiu, M.; Wang, D.; Liang, W.; Liu, L.; Zhang, Y.; Chen, X.; Sang, D.K.; Xing, C.; Li, Z.; Dong, B.; et al. Novel concept of the smart NIR-light–controlled drug release of black phosphorus nanostructure for cancer therapy. *Proc. Natl. Acad. Sci. USA* **2018**, *115*, 501–506. [CrossRef]
37. Wilson, K.; Homan, K.; Emelianov, S. Biomedical photoacoustics beyond thermal expansion using triggered nanodroplet vaporization for contrast-enhanced imaging. *Nat. Commun.* **2012**, *3*, 618. [CrossRef]

38. Fisher, D.G.; Price, R.J. Recent Advances in the Use of Focused Ultrasound for Magnetic Resonance Image-Guided Therapeutic Nanoparticle Delivery to the Central Nervous System. *Front. Pharmacol.* **2019**, *10*, 1–14. [CrossRef]
39. Choi, S.K. Photoactivation Strategies for Therapeutic Release in Nanodelivery Systems. *Adv. Ther.* **2020**, *3*, 2000117. [CrossRef]
40. Geisow, M.J.; Evans, W.H. pH in the endosome: Measurements during pinocytosis and receptor-mediated endocytosis. *Exp. Cell Res.* **1984**, *150*, 36–46. [CrossRef]
41. Chan, P.; Lovrić, J.; Warwicker, J. Subcellular pH and predicted pH-dependent features of proteins. *Proteomics* **2006**, *6*, 3494–3501. [CrossRef]
42. Geisow, M.J. Fluorescein conjugates as indicators of subcellular pH: A critical evaluation. *Exp. Cell Res.* **1984**, *150*, 29–35. [CrossRef]
43. Feazell, R.P.; Nakayama-Ratchford, N.; Dai, H.; Lippard, S.J. Soluble Single-Walled Carbon Nanotubes as Longboat Delivery Systems for Platinum(IV) Anticancer Drug Design. *J. Am. Chem. Soc.* **2007**, *129*, 8438–8439. [CrossRef] [PubMed]
44. Dubowchik, G.M.; Walker, M.A. Receptor-mediated and enzyme-dependent targeting of cytotoxic anticancer drugs. *Pharmacol. Therap.* **1999**, *83*, 67–123. [CrossRef]
45. Chen, D.; Yang, D.; Dougherty, C.A.; Lu, W.; Wu, H.; He, X.; Cai, T.; Van Dort, M.E.; Ross, B.D.; Hong, H. In Vivo Targeting and Positron Emission Tomography Imaging of Tumor with Intrinsically Radioactive Metal–Organic Frameworks Nanomaterials. *ACS Nano* **2017**, *11*, 4315–4327. [CrossRef]
46. Li, Z.; Dong, K.; Huang, S.; Ju, E.; Liu, Z.; Yin, M.; Ren, J.; Qu, X. A Smart Nanoassembly for Multistage Targeted Drug Delivery and Magnetic Resonance Imaging. *Adv. Funct. Mater.* **2014**, *24*, 3612–3620. [CrossRef]
47. Li, H.; Zhao, Y.; Jia, Y.; Qu, C.; Li, J. Covalently assembled dopamine nanoparticle as an intrinsic photosensitizer and pH-responsive nanocarrier for potential application in anticancer therapy. *Chem. Commun.* **2019**, *55*, 15057–15060. [CrossRef]
48. Zhou, H.; Qian, W.; Uckun, F.M.; Wang, L.; Wang, Y.A.; Chen, H.; Kooby, D.; Yu, Q.; Lipowska, M.; Staley, C.A.; et al. IGF1 Receptor Targeted Theranostic Nanoparticles for Targeted and Image-Guided Therapy of Pancreatic Cancer. *ACS Nano* **2015**, *9*, 7976–7991. [CrossRef]
49. Liu, X.; Wu, M.; Hu, Q.; Bai, H.; Zhang, S.; Shen, Y.; Tang, G.; Ping, Y. Redox-Activated Light-Up Nanomicelle for Precise Imaging-Guided Cancer Therapy and Real-Time Pharmacokinetic Monitoring. *ACS Nano* **2016**, *10*, 11385–11396. [CrossRef]
50. Ojima, I. Guided Molecular Missiles for Tumor-Targeting Chemotherapy;Case Studies Using the Second-Generation Taxoids as Warheads. *Acc. Chem. Res.* **2008**, *41*, 108–119. [CrossRef]
51. Sun, Z.; Liu, G.; Hu, J.; Liu, S. Photo- and Reduction-Responsive Polymersomes for Programmed Release of Small and Macromolecular Payloads. *Biomacromolecules* **2018**, *19*, 2071–2081. [CrossRef]
52. Huang, B.; Tang, S.; Desai, A.; Cheng, X.-m.; Kotlyar, A.; Spek, A.V.D.; Thomas, T.P.; Baker, J.R., Jr. Human plasma-mediated hypoxic activation of indolequinone-based naloxone pro-drugs. *Bioorg. Med. Chem. Lett.* **2009**, *19*, 5016–5020. [CrossRef] [PubMed]
53. Huang, B.; Desai, A.; Tang, S.; Thomas, T.P.; Baker, J.R. The Synthesis of a c(RGDyK) Targeted SN38 Prodrug with an Indolequinone Structure for Bioreductive Drug Release. *Org. Lett.* **2010**, *12*, 1384–1387. [CrossRef] [PubMed]
54. Naughton, D.P. Drug targeting to hypoxic tissue using self-inactivating bioreductive delivery systems. *Adv. Drug Deliv. Rev.* **2001**, *53*, 229–233. [CrossRef]
55. Dhar, S.; Liu, Z.; Thomale, J.; Dai, H.; Lippard, S.J. Targeted Single-Wall Carbon Nanotube-Mediated Pt(IV) Prodrug Delivery Using Folate as a Homing Device. *J. Am. Chem. Soc.* **2008**, *130*, 11467–11476. [CrossRef] [PubMed]
56. Kaminskas, L.M.; Kelly, B.D.; McLeod, V.M.; Sberna, G.; Boyd, B.J.; Owen, D.J.; Porter, C.J.H. Capping Methotrexate α-Carboxyl Groups Enhances Systemic Exposure and Retains the Cytotoxicity of Drug Conjugated PEGylated Polylysine Dendrimers. *Mol. Pharm.* **2011**, *8*, 338–349. [CrossRef] [PubMed]
57. Kaminskas, L.M.; Kelly, B.D.; McLeod, V.M.; Boyd, B.J.; Krippner, G.Y.; Williams, E.D.; Porter, C.J.H. Pharmacokinetics and Tumor Disposition of PEGylated, Methotrexate Conjugated Poly-l-lysine Dendrimers. *Mol. Pharm.* **2009**, *6*, 1190–1204. [CrossRef]
58. Homma, A.; Sato, H.; Okamachi, A.; Emura, T.; Ishizawa, T.; Kato, T.; Matsuura, T.; Sato, S.; Tamura, T.; Higuchi, Y.; et al. Novel hyaluronic acid-methotrexate conjugates for osteoarthritis treatment. *Bioorg. Med. Chem.* **2009**, *17*, 4647–4656. [CrossRef]

59. Yan, B.; Boyer, J.-C.; Branda, N.R.; Zhao, Y. Near-Infrared Light-Triggered Dissociation of Block Copolymer Micelles Using Upconverting Nanoparticles. *J. Am. Chem. Soc.* **2011**, *133*, 19714–19717. [CrossRef]
60. Zhang, Y.; Lu, G.; Yu, Y.; Zhang, H.; Gao, J.; Sun, Z.; Lu, Y.; Zou, H. NIR-responsive copolymer upconversion nanocomposites for triggered drug release in vitro and in vivo. *ACS Appl. Bio Mater.* **2019**, *2*, 495–503. [CrossRef]
61. Zhao, H.; Hu, W.; Ma, H.; Jiang, R.; Tang, Y.; Ji, Y.; Lu, X.; Hou, B.; Deng, W.; Huang, W.; et al. Photo-Induced Charge-Variable Conjugated Polyelectrolyte Brushes Encapsulating Upconversion Nanoparticles for Promoted siRNA Release and Collaborative Photodynamic Therapy under NIR Light Irradiation. *Adv. Funct. Mater.* **2017**, *27*, 1702592. [CrossRef]
62. Zhong, Y.; Wang, C.; Cheng, L.; Meng, F.; Zhong, Z.; Liu, Z. Gold Nanorod-Cored Biodegradable Micelles as a Robust and Remotely Controllable Doxorubicin Release System for Potent Inhibition of Drug-Sensitive and -Resistant Cancer Cells. *Biomacromolecules* **2013**, *14*, 2411–2419. [CrossRef] [PubMed]
63. Zhang, Z.; Wang, J.; Nie, X.; Wen, T.; Ji, Y.; Wu, X.; Zhao, Y.; Chen, C. Near Infrared Laser-Induced Targeted Cancer Therapy Using Thermoresponsive Polymer Encapsulated Gold Nanorods. *J. Am. Chem. Soc.* **2014**, *136*, 7317–7326. [CrossRef] [PubMed]
64. Shi, B.; Ren, N.; Gu, L.; Xu, G.; Wang, R.; Zhu, T.; Zhu, Y.; Fan, C.; Zhao, C.; Tian, H. Theranostic Nanoplatform with Hydrogen Sulfide Activatable NIR Responsiveness for Imaging-Guided On-Demand Drug Release. *Angew. Chem. Int. Ed.* **2019**, *58*, 16826–16830. [CrossRef] [PubMed]
65. Saravanakumar, G.; Lee, J.; Kim, J.; Kim, W.J. Visible light-induced singlet oxygen-mediated intracellular disassembly of polymeric micelles co-loaded with a photosensitizer and an anticancer drug for enhanced photodynamic therapy. *Chem. Commun.* **2015**, *51*, 9995–9998. [CrossRef]
66. Brega, V.; Scaletti, F.; Zhang, X.; Wang, L.-S.; Li, P.; Xu, Q.; Rotello, V.M.; Thomas, S.W. Polymer Amphiphiles for Photoregulated Anticancer Drug Delivery. *ACS Appl. Mater. Interfaces* **2019**, *11*, 2814–2820. [CrossRef]
67. Li, Y.; Wang, S.; Huang, Y.; Chen, Y.; Wu, W.; Liu, Y.; Zhang, J.; Feng, Y.; Jiang, X.; Gou, M. Light-activated drug release from prodrug nanoassemblies by structure destruction. *Chem. Commun.* **2019**, *55*, 13128–13131. [CrossRef]
68. Hernández-Montoto, A.; Gorbe, M.; Llopis-Lorente, A.; Terrés, J.M.; Montes, R.; Cao-Milán, R.; Díaz de Greñu, B.; Alfonso, M.; Orzaez, M.; Marcos, M.D.; et al. A NIR light-triggered drug delivery system using core–shell gold nanostars–mesoporous silica nanoparticles based on multiphoton absorption photo-dissociation of 2-nitrobenzyl PEG. *Chem. Commun.* **2019**, *55*, 9039–9042. [CrossRef]
69. He, S.; Krippes, K.; Ritz, S.; Chen, Z.; Best, A.; Butt, H.-J.; Mailänder, V.; Wu, S. Ultralow-intensity near-infrared light induces drug delivery by upconverting nanoparticles. *Chem. Commun.* **2015**, *51*, 431–434. [CrossRef]
70. Wang, D.; Wu, S. Red-Light-Responsive Supramolecular Valves for Photocontrolled Drug Release from Mesoporous Nanoparticles. *Langmuir* **2016**, *32*, 632–636. [CrossRef]
71. Liu, J.; Bu, W.; Pan, L.; Shi, J. NIR-Triggered Anticancer Drug Delivery by Upconverting Nanoparticles with Integrated Azobenzene-Modified Mesoporous Silica. *Angew. Chem. Int. Ed.* **2013**, *52*, 4375–4379. [CrossRef]
72. Li, M.; Yan, H.; Teh, C.; Korzh, V.; Zhao, Y. NIR-triggered drug release from switchable rotaxane-functionalized silica-covered Au nanorods. *Chem. Commun.* **2014**, *50*, 9745–9748. [CrossRef] [PubMed]
73. Lv, R.; Yang, P.; He, F.; Gai, S.; Li, C.; Dai, Y.; Yang, G.; Lin, J. A Yolk-like Multifunctional Platform for Multimodal Imaging and Synergistic Therapy Triggered by a Single Near-Infrared Light. *ACS Nano* **2015**, *9*, 1630–1647. [CrossRef] [PubMed]
74. Yagüe, C.; Arruebo, M.; Santamaria, J. NIR-enhanced drug release from porous Au/SiO_2 nanoparticles. *Chem. Commun.* **2010**, *46*, 7513–7515. [CrossRef]
75. Chan, J.M.; Zhang, L.; Tong, R.; Ghosh, D.; Gao, W.; Liao, G.; Yuet, K.P.; Gray, D.; Rhee, J.-W.; Cheng, J.; et al. Spatiotemporal controlled delivery of nanoparticles to injured vasculature. *Proc. Natl. Acad. Sci. USA* **2010**, *107*, 2213–2218. [CrossRef] [PubMed]
76. Choi, S.K. Mechanistic Basis of Light Induced Cytotoxicity of Photoactive Nanomaterials. *NanoImpact* **2016**, *3-4*, 81–89. [CrossRef]
77. Xue, X.; Zhao, Y.; Dai, L.; Zhang, X.; Hao, X.; Zhang, C.; Huo, S.; Liu, J.; Liu, C.; Kumar, A.; et al. Spatiotemporal Drug Release Visualized through a Drug Delivery System with Tunable Aggregation-Induced Emission. *Adv. Mater.* **2014**, *26*, 712–717. [CrossRef]

78. Deepagan, V.G.; You, D.G.; Um, W.; Ko, H.; Kwon, S.; Choi, K.Y.; Yi, G.-R.; Lee, J.Y.; Lee, D.S.; Kim, K.; et al. Long-Circulating Au-TiO2 Nanocomposite as a Sonosensitizer for ROS-Mediated Eradication of Cancer. *Nano Lett.* **2016**, *16*, 6257–6264. [CrossRef]
79. Wong, P.T.; Tang, S.; Cannon, J.; Mukherjee, J.; Isham, D.; Gam, K.; Payne, M.; Yanik, S.A.; Baker, J.R.; Choi, S.K. A Thioacetal Photocage Designed for Dual Release: Application in the Quantitation of Therapeutic Release by Synchronous Reporter Decaging. *ChemBioChem* **2017**, *18*, 126–135. [CrossRef]
80. Choi, S.K. (Ed.) Chapter 1—Light sources for photonanotechnology. In *Photonanotechnology for Therapeutics and Imaging*; Elsevier: Amsterdam, The Netherlands, 2020; pp. 1–21.
81. Agasti, S.S.; Chompoosor, A.; You, C.-C.; Ghosh, P.; Kim, C.K.; Rotello, V.M. Photoregulated Release of Caged Anticancer Drugs from Gold Nanoparticles. *J. Am. Chem. Soc.* **2009**, *131*, 5728–5729. [CrossRef]
82. Mahmoodi, M.M.; Abate-Pella, D.; Pundsack, T.J.; Palsuledesai, C.C.; Goff, P.C.; Blank, D.A.; Distefano, M.D. Nitrodibenzofuran: A One- and Two-Photon Sensitive Protecting Group That Is Superior to Brominated Hydroxycoumarin for Thiol Caging in Peptides. *J. Am. Chem. Soc.* **2016**, *138*, 5848–5859. [CrossRef]
83. Jin, Q.; Mitschang, F.; Agarwal, S. Biocompatible Drug Delivery System for Photo-Triggered Controlled Release of 5-Fluorouracil. *Biomacromolecules* **2011**, *12*, 3684–3691. [CrossRef] [PubMed]
84. Vuilleumier, J.; Gaulier, G.; De Matos, R.; Mugnier, Y.; Campargue, G.; Wolf, J.-P.; Bonacina, L.; Gerber-Lemaire, S. Photocontrolled Release of the Anticancer Drug Chlorambucil with Caged Harmonic Nanoparticles. *Helv. Chim. Acta* **2020**, *103*, e1900251. [CrossRef]
85. Gore, S.; Ukhanov, K.; Herbivo, C.; Asad, N.; Bobkov, Y.V.; Martens, J.R.; Dore, T.M. Photoactivatable Odorants for Chemosensory Research. *ACS Chem. Biol.* **2020**, *15*, 2516–2528. [CrossRef] [PubMed]
86. Zhu, Y.; Pavlos, C.M.; Toscano, J.P.; Dore, T.M. 8-Bromo-7-hydroxyquinoline as a Photoremovable Protecting Group for Physiological Use: Mechanism and Scope. *J. Am. Chem. Soc.* **2006**, *128*, 4267–4276. [CrossRef]
87. Yu, G.; Yu, W.; Mao, Z.; Gao, C.; Huang, F. A Pillararene-Based Ternary Drug-Delivery System with Photocontrolled Anticancer Drug Release. *Small* **2015**, *11*, 919–925. [CrossRef]
88. Janett, E.; Bernardinelli, Y.; Müller, D.; Bochet, C.G. Synthesis of FMRFaNV, a Photoreleasable Caged Transmitter Designed to Study Neuron–Glia Interactions in the Central Nervous System. *Bioconjug. Chem.* **2015**, *26*, 2408–2418. [CrossRef]
89. Liu, Z.; Lin, Q.; Huang, Q.; Liu, H.; Bao, C.; Zhang, W.; Zhong, X.; Zhu, L. Semiconductor quantum dots photosensitizing release of anticancer drug. *Chem. Commun.* **2011**, *47*, 1482–1484. [CrossRef]
90. Dcona, M.M.; Yu, Q.; Capobianco, J.A.; Hartman, M.C.T. Near infrared light mediated release of doxorubicin using upconversion nanoparticles. *Chem. Commun.* **2015**, *51*, 8477–8479. [CrossRef]
91. Choi, S.K.; Verma, M.; Silpe, J.; Moody, R.E.; Tang, K.; Hanson, J.J.; Baker, J.R., Jr. A photochemical approach for controlled drug release in targeted drug delivery. *Bioorg. Med. Chem.* **2012**, *20*, 1281–1290. [CrossRef]
92. Choi, S.K.; Thomas, T.P.; Li, M.-H.; Desai, A.; Kotlyar, A.; Baker, J.R. Photochemical release of methotrexate from folate receptor-targeting PAMAM dendrimer nanoconjugate. *Photochem. Photobiol. Sci.* **2012**, *11*, 653–660. [CrossRef]
93. Xu, C.; Li, H.; Zhang, K.; Binzel, D.W.; Yin, H.; Chiu, W.; Guo, P. Photo-controlled release of paclitaxel and model drugs from RNA pyramids. *Nano Res.* **2019**, *12*, 41–48. [CrossRef] [PubMed]
94. Hu, X.; Tian, J.; Liu, T.; Zhang, G.; Liu, S. Photo-Triggered Release of Caged Camptothecin Prodrugs from Dually Responsive Shell Cross-Linked Micelles. *Macromolecules* **2013**, *46*, 6243–6256. [CrossRef]
95. Huang, L.; Zhao, Y.; Zhang, H.; Huang, K.; Yang, J.; Han, G. Expanding Anti-Stokes Shifting in Triplet–Triplet Annihilation Upconversion for In Vivo Anticancer Prodrug Activation. *Angew. Chem. Int. Ed.* **2017**, *56*, 14400–14404. [CrossRef] [PubMed]
96. Li, X.; Mu, J.; Liu, F.; Tan, E.W.P.; Khezri, B.; Webster, R.D.; Yeow, E.K.L.; Xing, B. Human Transport Protein Carrier for Controlled Photoactivation of Antitumor Prodrug and Real-Time Intracellular Tumor Imaging. *Bioconjug. Chem.* **2015**, *26*, 955–961. [CrossRef] [PubMed]
97. Song, H.; Li, W.; Qi, R.; Yan, L.; Jing, X.; Zheng, M.; Xiao, H. Delivering a photosensitive transplatin prodrug to overcome cisplatin drug resistance. *Chem. Commun.* **2015**, *51*, 11493–11495. [CrossRef] [PubMed]
98. Dai, Y.; Xiao, H.; Liu, J.; Yuan, Q.; Ma, P.A.; Yang, D.; Li, C.; Cheng, Z.; Hou, Z.; Yang, P.; et al. In Vivo Multimodality Imaging and Cancer Therapy by Near-Infrared Light-Triggered trans-Platinum Pro-Drug-Conjugated Upconverison Nanoparticles. *J. Am. Chem. Soc.* **2013**, *135*, 18920–18929. [CrossRef]

99. Shi, Y.; Truong, V.X.; Kulkarni, K.; Qu, Y.; Simon, G.P.; Boyd, R.L.; Perlmutter, P.; Lithgow, T.; Forsythe, J.S. Light-triggered release of ciprofloxacin from an in situ forming click hydrogel for antibacterial wound dressings. *J. Mater. Chem. B* **2015**, *3*, 8771–8774. [CrossRef] [PubMed]
100. Wong, P.T.; Tang, S.; Tang, K.; Coulter, A.; Mukherjee, J.; Gam, K.; Baker, J.R.; Choi, S.K. A lipopolysaccharide binding heteromultivalent dendrimer nanoplatform for Gram negative cell targeting. *J. Mater. Chem. B* **2015**, *3*, 1149–1156. [CrossRef]
101. Han, G.; You, C.-C.; Kim, B.-j.; Turingan, R.S.; Forbes, N.S.; Martin, C.T.; Rotello, V.M. Light-Regulated Release of DNA and Its Delivery to Nuclei by Means of Photolabile Gold Nanoparticles. *Angew. Chem. Int. Ed.* **2006**, *45*, 3165–3169. [CrossRef]
102. Brown, P.K.; Qureshi, A.T.; Moll, A.N.; Hayes, D.J.; Monroe, W.T. Silver Nanoscale Antisense Drug Delivery System for Photoactivated Gene Silencing. *ACS Nano* **2013**, *7*, 2948–2959. [CrossRef]
103. Jayakumar, M.K.G.; Bansal, A.; Huang, K.; Yao, R.; Li, B.N.; Zhang, Y. Near-Infrared-Light-Based Nano-Platform Boosts Endosomal Escape and Controls Gene Knockdown in Vivo. *ACS Nano* **2014**, *8*, 4848–4858. [CrossRef] [PubMed]
104. Pan, Y.; Yang, J.; Luan, X.; Liu, X.; Li, X.; Yang, J.; Huang, T.; Sun, L.; Wang, Y.; Lin, Y.; et al. Near-infrared upconversion–activated CRISPR-Cas9 system: A remote-controlled gene editing platform. *Sci. Adv.* **2019**, *5*, eaav7199. [CrossRef]
105. Pierri, A.E.; Huang, P.-J.; Garcia, J.V.; Stanfill, J.G.; Chui, M.; Wu, G.; Zheng, N.; Ford, P.C. A photoCORM nanocarrier for CO release using NIR light. *Chem. Commun.* **2015**, *51*, 2072–2075. [CrossRef] [PubMed]
106. Fraix, A.; Kandoth, N.; Manet, I.; Cardile, V.; Graziano, A.C.E.; Gref, R.; Sortino, S. An engineered nanoplatform for bimodal anticancer phototherapy with dual-color fluorescence detection of sensitizers. *Chem. Commun.* **2013**, *49*, 4459–4461. [CrossRef]
107. Fowley, C.; McHale, A.P.; McCaughan, B.; Fraix, A.; Sortino, S.; Callan, J.F. Carbon quantum dot–NO photoreleaser nanohybrids for two-photon phototherapy of hypoxic tumors. *Chem. Commun.* **2015**, *51*, 81–84. [CrossRef] [PubMed]
108. Guo, M.; Xiang, H.-J.; Wang, Y.; Zhang, Q.-L.; An, L.; Yang, S.-P.; Ma, Y.; Wang, Y.; Liu, J.-G. Ruthenium nitrosyl functionalized graphene quantum dots as an efficient nanoplatform for NIR-light-controlled and mitochondria-targeted delivery of nitric oxide combined with photothermal therapy. *Chem. Commun.* **2017**, *53*, 3253–3256. [CrossRef]
109. Xiang, H.-J.; An, L.; Tang, W.-W.; Yang, S.-P.; Liu, J.-G. Photo-controlled targeted intracellular delivery of both nitric oxide and singlet oxygen using a fluorescence-trackable ruthenium nitrosyl functional nanoplatform. *Chem. Commun.* **2015**, *51*, 2555–2558. [CrossRef]
110. Li, S.; Liu, R.; Jiang, X.; Qiu, Y.; Song, X.; Huang, G.; Fu, N.; Lin, L.; Song, J.; Chen, X.; et al. Near-Infrared Light-Triggered Sulfur Dioxide Gas Therapy of Cancer. *ACS Nano* **2019**, *13*, 2103–2113. [CrossRef]
111. Chen, W.; Chen, M.; Zang, Q.; Wang, L.; Tang, F.; Han, Y.; Yang, C.; Deng, L.; Liu, Y.-N. NIR light controlled release of caged hydrogen sulfide based on upconversion nanoparticles. *Chem. Commun.* **2015**, *51*, 9193–9196. [CrossRef]
112. Chen, W.; Ni, D.; Rosenkrans, Z.T.; Cao, T.; Cai, W. Smart H2S-Triggered/Therapeutic System (SHTS)-Based Nanomedicine. *Adv. Sci.* **2019**, *6*, 1901724. [CrossRef]
113. Nani, R.R.; Gorka, A.P.; Nagaya, T.; Kobayashi, H.; Schnermann, M.J. Near-IR Light-Mediated Cleavage of Antibody–Drug Conjugates Using Cyanine Photocages. *Angew. Chem. Int. Ed.* **2015**, *54*, 13635–13638. [CrossRef] [PubMed]
114. Gorka, A.P.; Nani, R.R.; Zhu, J.; Mackem, S.; Schnermann, M.J. A Near-IR Uncaging Strategy Based on Cyanine Photochemistry. *J. Am. Chem. Soc.* **2014**, *136*, 14153–14159. [CrossRef]
115. Xiang, J.; Ge, F.; Yu, B.; Yan, Q.; Shi, F.; Zhao, Y. Nanocomplexes of Photolabile Polyelectrolyte and Upconversion Nanoparticles for Near-Infrared Light-Triggered Payload Release. *ACS Appl. Mater. Interfaces* **2018**, *10*, 20790–20800. [CrossRef] [PubMed]
116. Song, H.; Kang, X.; Sun, J.; Jing, X.; Wang, Z.; Yan, L.; Qi, R.; Zheng, M. Nanoparticle delivery of sterically hindered platinum(iv) prodrugs shows 100 times higher potency than that of cisplatin upon light activation. *Chem. Commun.* **2016**, *52*, 2281–2283. [CrossRef] [PubMed]
117. Chandra, B.; Mallik, S.; Srivastava, D.K. Design of photocleavable lipids and their application in liposomal "uncorking". *Chem. Commun.* **2005**, 3021–3023. [CrossRef] [PubMed]

118. Reeßing, F.; Stuart, M.C.A.; Samplonius, D.F.; Dierckx, R.A.J.O.; Feringa, B.L.; Helfrich, W.; Szymanski, W. A light-responsive liposomal agent for MRI contrast enhancement and monitoring of cargo delivery. *Chem. Commun.* **2019**, *55*, 10784–10787. [CrossRef]
119. Wu, H.; Dong, J.; Li, C.; Liu, Y.; Feng, N.; Xu, L.; Zhan, X.; Yang, H.; Wang, G. Multi-responsive nitrobenzene-based amphiphilic random copolymer assemblies. *Chem. Commun.* **2013**, *49*, 3516–3518. [CrossRef]
120. Patil, N.G.; Basutkar, N.B.; Ambade, A.V. Visible light-triggered disruption of micelles of an amphiphilic block copolymer with BODIPY at the junction. *Chem. Commun.* **2015**, *51*, 17708–17711. [CrossRef]
121. Li, Y.; Qian, Y.; Liu, T.; Zhang, G.; Liu, S. Light-Triggered Concomitant Enhancement of Magnetic Resonance Imaging Contrast Performance and Drug Release Rate of Functionalized Amphiphilic Diblock Copolymer Micelles. *Biomacromolecules* **2012**, *13*, 3877–3886. [CrossRef]
122. Yang, J.; Song, J.-I.; Song, Q.; Rho, J.Y.; Mansfield, E.D.H.; Hall, S.C.L.; Sambrook, M.; Huang, F.; Perrier, S. Hierarchical Self-Assembled Photo-Responsive Tubisomes from a Cyclic Peptide-Bridged Amphiphilic Block Copolymer. *Angew. Chem. Int. Ed.* **2020**, *59*, 8860–8863. [CrossRef]
123. Sun, F.; Zhang, P.; Liu, Y.; Lu, C.; Qiu, Y.; Mu, H.; Duan, J. A photo-controlled hyaluronan-based drug delivery nanosystem for cancer therapy. *Carbohydr. Polym.* **2019**, *206*, 309–318. [CrossRef] [PubMed]
124. Yang, L.; Sun, H.; Liu, Y.; Hou, W.; Yang, Y.; Cai, R.; Cui, C.; Zhang, P.; Pan, X.; Li, X.; et al. Self-Assembled Aptamer-Grafted Hyperbranched Polymer Nanocarrier for Targeted and Photoresponsive Drug Delivery. *Angew. Chem. Int. Ed.* **2018**, *57*, 17048–17052. [CrossRef] [PubMed]
125. Pasparakis, G.; Manouras, T.; Vamvakaki, M.; Argitis, P. Harnessing photochemical internalization with dual degradable nanoparticles for combinatorial photo–chemotherapy. *Nat. Commun.* **2014**, *5*, 3623. [CrossRef]
126. Zhao, X.; Qi, M.; Liang, S.; Tian, K.; Zhou, T.; Jia, X.; Li, J.; Liu, P. Synthesis of Photo- and pH Dual-Sensitive Amphiphilic Copolymer PEG43-b-P(AA76-co-NBA35-co-tBA9) and Its Micellization as Leakage-Free Drug Delivery System for UV-Triggered Intracellular Delivery of Doxorubicin. *ACS Appl. Mater. Interfaces* **2016**, *8*, 22127–22134. [CrossRef] [PubMed]
127. Abebe Alemayehu, Y.; Tewabe Gebeyehu, B.; Cheng, C.-C. Photosensitive Supramolecular Micelles with Complementary Hydrogen Bonding Motifs to Improve the Efficacy of Cancer Chemotherapy. *Biomacromolecules* **2019**, *20*, 4535–4545. [CrossRef]
128. Liang, X.; Yue, X.; Dai, Z.; Kikuchi, J.-i. Photoresponsive liposomal nanohybrid cerasomes. *Chem. Commun.* **2011**, *47*, 4751–4753. [CrossRef]
129. Poelma, S.O.; Oh, S.S.; Helmy, S.; Knight, A.S.; Burnett, G.L.; Soh, H.T.; Hawker, C.J.; Read de Alaniz, J. Controlled drug release to cancer cells from modular one-photon visible light-responsive micellar system. *Chem. Commun.* **2016**, *52*, 10525–10528. [CrossRef]
130. Namazi, H.; Jafarirad, S. Invitro Photo-Controlled Drug Release System Based on Amphiphilic Linear-Dendritic Diblock Copolymers; Self-Assembly Behavior and Application as Nanocarrier. *J. Pharm. Pharm. Sci.* **2011**, *14*, 162–180. [CrossRef]
131. Yan, Q.; Xin, Y.; Zhou, R.; Yin, Y.; Yuan, J. Light-controlled smart nanotubes based on the orthogonal assembly of two homopolymers. *Chem. Commun.* **2011**, *47*, 9594–9596. [CrossRef]
132. Li, F.-Q.; Yu, Q.-L.; Liu, Y.-H.; Yu, H.-J.; Chen, Y.; Liu, Y. Highly efficient photocontrolled targeted delivery of siRNA by a cyclodextrin-based supramolecular nanoassembly. *Chem. Commun.* **2020**, *56*, 3907–3910. [CrossRef]
133. Huang, Y.; Shen, L.; Guo, D.; Yasen, W.; Wu, Y.; Su, Y.; Chen, D.; Qiu, F.; Yan, D.; Zhu, X. A NIR-triggered gatekeeper of supramolecular conjugated unimicelles with two-photon absorption for controlled drug release. *Chem. Commun.* **2019**, *55*, 6735–6738. [CrossRef] [PubMed]
134. Zhao, T.; Wang, P.; Li, Q.; Al-Khalaf, A.A.; Hozzein, W.N.; Zhang, F.; Li, X.; Zhao, D. Near-Infrared Triggered Decomposition of Nanocapsules with High Tumor Accumulation and Stimuli Responsive Fast Elimination. *Angew. Chem. Int. Ed.* **2018**, *57*, 2611–2615. [CrossRef] [PubMed]
135. Peng, K.; Tomatsu, I.; Kros, A. Light controlled protein release from a supramolecular hydrogel. *Chem. Commun.* **2010**, *46*, 4094–4096. [CrossRef]
136. Karcher, J.; Pianowski, Z.L. Photocontrol of Drug Release from Supramolecular Hydrogels with Green Light. *Chem. Eur. J.* **2018**, *24*, 11605–11610. [CrossRef] [PubMed]

137. Roth Stefaniak, K.; Epley, C.C.; Novak, J.J.; McAndrew, M.L.; Cornell, H.D.; Zhu, J.; McDaniel, D.K.; Davis, J.L.; Allen, I.C.; Morris, A.J.; et al. Photo-triggered release of 5-fluorouracil from a MOF drug delivery vehicle. *Chem. Commun.* **2018**, *54*, 7617–7620. [CrossRef] [PubMed]
138. Möller, N.; Hellwig, T.; Stricker, L.; Engel, S.; Fallnich, C.; Ravoo, B.J. Near-infrared photoswitching of cyclodextrin–guest complexes using lanthanide-doped LiYF4 upconversion nanoparticles. *Chem. Commun.* **2017**, *53*, 240–243. [CrossRef] [PubMed]
139. Zhang, C.; Sun, W.; Wang, Y.; Xu, F.; Qu, J.; Xia, J.; Shen, M.; Shi, X. Gd-/CuS-Loaded Functional Nanogels for MR/PA Imaging-Guided Tumor-Targeted Photothermal Therapy. *ACS Appl. Mater. Interfaces* **2020**, *12*, 9107–9117. [CrossRef]
140. Sloand, J.N.; Nguyen, T.T.; Zinck, S.A.; Cook, E.C.; Zimudzi, T.J.; Showalter, S.A.; Glick, A.B.; Simon, J.C.; Medina, S.H. Ultrasound-Guided Cytosolic Protein Delivery via Transient Fluorous Masks. *ACS Nano* **2020**, *14*, 4061–4073. [CrossRef]
141. Chen, J.; Ratnayaka, S.; Alford, A.; Kozlovskaya, V.; Liu, F.; Xue, B.; Hoyt, K.; Kharlampieva, E. Theranostic Multilayer Capsules for Ultrasound Imaging and Guided Drug Delivery. *ACS Nano* **2017**, *11*, 3135–3146. [CrossRef]
142. Knežević, N.Ž.; Trewyn, B.G.; Lin, V.S.Y. Functionalized mesoporous silica nanoparticle-based visible light responsive controlled release delivery system. *Chem. Commun.* **2011**, *47*, 2817–2819. [CrossRef]
143. Ma, N.; Wang, W.-J.; Chen, S.; Wang, X.-S.; Wang, X.-Q.; Wang, S.-B.; Zhu, J.-Y.; Cheng, S.-X.; Zhang, X.-Z. Cucurbit[8]uril-mediated supramolecular photoswitching for self-preservation of mesoporous silica nanoparticle delivery system. *Chem. Commun.* **2015**, *51*, 12970–12973. [CrossRef] [PubMed]
144. Lai, J.; Mu, X.; Xu, Y.; Wu, X.; Wu, C.; Li, C.; Chen, J.; Zhao, Y. Light-responsive nanogated ensemble based on polymer grafted mesoporous silica hybrid nanoparticles. *Chem. Commun.* **2010**, *46*, 7370–7372. [CrossRef] [PubMed]
145. Zhao, Q.; Wang, Y.; Yan, Y.; Huang, J. Smart Nanocarrier: Self-Assembly of Bacteria-like Vesicles with Photoswitchable Cilia. *ACS Nano* **2014**, *8*, 11341–11349. [CrossRef] [PubMed]
146. Yao, C.; Wang, P.; Li, X.; Hu, X.; Hou, J.; Wang, L.; Zhang, F. Near-Infrared-Triggered Azobenzene-Liposome/Upconversion Nanoparticle Hybrid Vesicles for Remotely Controlled Drug Delivery to Overcome Cancer Multidrug Resistance. *Adv. Mater.* **2016**, *28*, 9341–9348. [CrossRef] [PubMed]
147. Beňová, E.; Zeleňák, V.; Halamová, D.; Almáši, M.; Petrul'ová, V.; Psotka, M.; Zeleňáková, A.; Bačkor, M.; Hornebecq, V. A drug delivery system based on switchable photo-controlled p-coumaric acid derivatives anchored on mesoporous silica. *J. Mater. Chem. B* **2017**, *5*, 817–825. [CrossRef] [PubMed]
148. Martinez-Cuezva, A.; Valero-Moya, S.; Alajarin, M.; Berna, J. Light-responsive peptide [2]rotaxanes as gatekeepers of mechanised nanocontainers. *Chem. Commun.* **2015**, *51*, 14501–14504. [CrossRef] [PubMed]
149. Wang, X.; Hu, J.; Liu, G.; Tian, J.; Wang, H.; Gong, M.; Liu, S. Reversibly Switching Bilayer Permeability and Release Modules of Photochromic Polymersomes Stabilized by Cooperative Noncovalent Interactions. *J. Am. Chem. Soc.* **2015**, *137*, 15262–15275. [CrossRef] [PubMed]
150. Senthilkumar, T.; Zhou, L.; Gu, Q.; Liu, L.; Lv, F.; Wang, S. Conjugated Polymer Nanoparticles with Appended Photo-Responsive Units for Controlled Drug Delivery, Release, and Imaging. *Angew. Chem. Int. Ed.* **2018**, *57*, 13114–13119. [CrossRef]
151. Yan, H.; Teh, C.; Sreejith, S.; Zhu, L.; Kwok, A.; Fang, W.; Ma, X.; Nguyen, K.T.; Korzh, V.; Zhao, Y. Functional Mesoporous Silica Nanoparticles for Photothermal-Controlled Drug Delivery In Vivo. *Angew. Chem. Int. Ed.* **2012**, *51*, 8373–8377. [CrossRef] [PubMed]
152. Yuan, Q.; Zhang, Y.; Chen, T.; Lu, D.; Zhao, Z.; Zhang, X.; Li, Z.; Yan, C.-H.; Tan, W. Photon-Manipulated Drug Release from a Mesoporous Nanocontainer Controlled by Azobenzene-Modified Nucleic Acid. *ACS Nano* **2012**, *6*, 6337–6344. [CrossRef] [PubMed]
153. Xu, J.; Liu, N.; Wu, D.; Gao, Z.; Song, Y.-Y.; Schmuki, P. Upconversion Nanoparticle-Assisted Payload Delivery from TiO2 under Near-Infrared Light Irradiation for Bacterial Inactivation. *ACS Nano* **2020**, *14*, 337–346. [CrossRef]
154. Winterbourn, C.C. Reconciling the chemistry and biology of reactive oxygen species. *Nat. Chem. Biol.* **2008**, *4*, 278–286. [CrossRef]
155. Lucky, S.S.; Soo, K.C.; Zhang, Y. Nanoparticles in Photodynamic Therapy. *Chem. Rev.* **2015**, *115*, 1990–2042. [CrossRef] [PubMed]

156. Lee, J.; Park, J.; Singha, K.; Kim, W.J. Mesoporous silica nanoparticle facilitated drug release through cascade photosensitizer activation and cleavage of singlet oxygen sensitive linker. *Chem. Commun.* **2013**, *49*, 1545–1547. [CrossRef] [PubMed]
157. Zhang, Y.; Huang, P.; Wang, D.; Chen, J.; Liu, W.; Hu, P.; Huang, M.; Chen, X.; Chen, Z. Near-infrared-triggered antibacterial and antifungal photodynamic therapy based on lanthanide-doped upconversion nanoparticles. *Nanoscale* **2018**, *10*, 15485–15495. [CrossRef] [PubMed]
158. Wu, W.; Shao, X.; Zhao, J.; Wu, M. Controllable Photodynamic Therapy Implemented by Regulating Singlet Oxygen Efficiency. *Adv. Sci.* **2017**, *4*, 1700113. [CrossRef]
159. Ji, C.; Gao, Q.; Dong, X.; Yin, W.; Gu, Z.; Gan, Z.; Zhao, Y.; Yin, M. A Size-Reducible Nanodrug with an Aggregation-Enhanced Photodynamic Effect for Deep Chemo-Photodynamic Therapy. *Angew. Chem. Int. Ed.* **2018**, *57*, 11384–11388. [CrossRef]
160. Mu, Q.; Jiang, G.; Chen, L.; Zhou, H.; Fourches, D.; Tropsha, A.; Yan, B. Chemical Basis of Interactions Between Engineered Nanoparticles and Biological Systems. *Chem. Rev.* **2014**, *114*, 7740–7781. [CrossRef]
161. Luo, L.; Guo, Y.; Yang, J.; Liu, Y.; Chu, S.; Kong, F.; Wang, Y.; Zou, Z. An efficient visible light controlled protein delivery system. *Chem. Commun.* **2011**, *47*, 11243–11245. [CrossRef]
162. Ye, Y.; Li, Y.; Fang, F. Upconversion nanoparticles conjugated with curcumin as a photosensitizer to inhibit methicillin-resistant Staphylococcus aureus in lung under near infrared light. *Int. J. Nanomed.* **2014**, *9*, 5157–5165. [CrossRef]
163. Li, S.; Cui, S.; Yin, D.; Zhu, Q.; Ma, Y.; Qian, Z.; Gu, Y. Dual antibacterial activities of a chitosan-modified upconversion photodynamic therapy system against drug-resistant bacteria in deep tissue. *Nanoscale* **2017**, *9*, 3912–3924. [CrossRef] [PubMed]
164. Pan, H.; Wang, S.; Xue, Y.; Cao, H.; Zhang, W. Light-controllable toxicity recovery from selenium-based amphiphiles. *Chem. Commun.* **2016**, *52*, 14208–14211. [CrossRef] [PubMed]
165. Wang, Y.; Tian, N.; Li, C.; Hou, Y.; Wang, X.; Zhou, Q. Incorporation of 7-dehydrocholesterol into liposomes as a simple, universal and efficient way to enhance anticancer activity by combining PDT and photoactivated chemotherapy. *Chem. Commun.* **2019**, *55*, 14081–14084. [CrossRef] [PubMed]
166. Pei, Q.; Hu, X.; Zheng, X.; Liu, S.; Li, Y.; Jing, X.; Xie, Z. Light-Activatable Red Blood Cell Membrane-Camouflaged Dimeric Prodrug Nanoparticles for Synergistic Photodynamic/Chemotherapy. *ACS Nano* **2018**, *12*, 1630–1641. [CrossRef] [PubMed]
167. Kim, K.; Lee, C.-S.; Na, K. Light-controlled reactive oxygen species (ROS)-producible polymeric micelles with simultaneous drug-release triggering and endo/lysosomal escape. *Chem. Commun.* **2016**, *52*, 2839–2842. [CrossRef] [PubMed]
168. Wan, Y.; Zheng, L.; Sun, Y.; Zhang, D. Multifunctional semiconducting polymer dots for imaging, detection, and photo-killing of bacteria. *J. Mater. Chem. B* **2014**, *2*, 4818–4825. [CrossRef]
169. Guo, S.; Liu, X.; Yao, C.; Lu, C.; Chen, Q.; Hu, X.-Y.; Wang, L. Photolysis of a bola-type supra-amphiphile promoted by water-soluble pillar[5]arene-induced assembly. *Chem. Commun.* **2016**, *52*, 10751–10754. [CrossRef]
170. Zhu, J.; Xiao, T.; Zhang, J.; Che, H.; Shi, Y.; Shi, X.; van Hest, J.C.M. Surface-Charge-Switchable Nanoclusters for Magnetic Resonance Imaging-Guided and Glutathione Depletion-Enhanced Photodynamic Therapy. *ACS Nano* **2020**, *14*, 11225–11237. [CrossRef]
171. Rout, B.; Liu, C.-H.; Wu, W.-C. Photosensitizer in lipid nanoparticle: A nano-scaled approach to antibacterial function. *Sci. Rep.* **2017**, *7*, 7892. [CrossRef]
172. Hamblin, M.R. Antimicrobial Photodynamic Therapy and Photodynamic Inactivation, or Killing Bugs with Dyes and Light—A Symposium-in-Print. *Photochem. Photobiol.* **2012**, *88*, 496–498. [CrossRef]
173. Nishiyama, N.; Morimoto, Y.; Jang, W.-D.; Kataoka, K. Design and development of dendrimer photosensitizer-incorporated polymeric micelles for enhanced photodynamic therapy. *Adv. Drug Deliv. Rev.* **2009**, *61*, 327–338. [CrossRef] [PubMed]
174. Celli, J.P.; Spring, B.Q.; Rizvi, I.; Evans, C.L.; Samkoe, K.S.; Verma, S.; Pogue, B.W.; Hasan, T. Imaging and Photodynamic Therapy: Mechanisms, Monitoring, and Optimization. *Chem. Rev.* **2010**, *110*, 2795–2838. [CrossRef] [PubMed]
175. Moussaron, A.; Youssef, Z.; Ben-Mihoub, A.; Vanderesse, R.; Frochot, C.; Acherar, S. Chapter 5—Dual imaging and photodynamic therapy anticancer theranostic nanoparticles. In *Photonanotechnology for Therapeutics and Imaging*; Choi, S.K., Ed.; Elsevier: Amsterdam, The Netherlands, 2020; pp. 105–146.

176. Xu, J.; Yu, S.; Wang, X.; Qian, Y.; Wu, W.; Zhang, S.; Zheng, B.; Wei, G.; Gao, S.; Cao, Z.; et al. High Affinity of Chlorin e6 to Immunoglobulin G for Intraoperative Fluorescence Image-Guided Cancer Photodynamic and Checkpoint Blockade Therapy. *ACS Nano* **2019**, *13*, 10242–10260. [CrossRef]
177. Zhang, H.; Liu, K.; Li, S.; Xin, X.; Yuan, S.; Ma, G.; Yan, X. Self-Assembled Minimalist Multifunctional Theranostic Nanoplatform for Magnetic Resonance Imaging-Guided Tumor Photodynamic Therapy. *ACS Nano* **2018**, *12*, 8266–8276. [CrossRef] [PubMed]
178. Yuan, Y.; Feng, G.; Qin, W.; Tang, B.Z.; Liu, B. Targeted and image-guided photodynamic cancer therapy based on organic nanoparticles with aggregation-induced emission characteristics. *Chem. Commun.* **2014**, *50*, 8757–8760. [CrossRef] [PubMed]
179. Li, M.; Gao, Y.; Yuan, Y.; Wu, Y.; Song, Z.; Tang, B.Z.; Liu, B.; Zheng, Q.C. One-Step Formulation of Targeted Aggregation-Induced Emission Dots for Image-Guided Photodynamic Therapy of Cholangiocarcinoma. *ACS Nano* **2017**, *11*, 3922–3932. [CrossRef]
180. Yang, Z.; Du, Y.; Sun, Q.; Peng, Y.; Wang, R.; Zhou, Y.; Wang, Y.; Zhang, C.; Qi, X. Albumin-Based Nanotheranostic Probe with Hypoxia Alleviating Potentiates Synchronous Multimodal Imaging and Phototherapy for Glioma. *ACS Nano* **2020**, *14*, 6191–6212. [CrossRef]
181. Liu, Y.; Bhattarai, P.; Dai, Z.; Chen, X. Photothermal therapy and photoacoustic imaging via nanotheranostics in fighting cancer. *Chem. Soc. Rev.* **2019**, *48*, 2053–2108. [CrossRef]
182. Fang, S.; Lin, J.; Li, C.; Huang, P.; Hou, W.; Zhang, C.; Liu, J.; Huang, S.; Luo, Y.; Fan, W.; et al. Dual-Stimuli Responsive Nanotheranostics for Multimodal Imaging Guided Trimodal Synergistic Therapy. *Small* **2017**, *13*, 1602580. [CrossRef]
183. Melancon, M.P.; Zhou, M.; Zhang, R.; Xiong, C.; Allen, P.; Wen, X.; Huang, Q.; Wallace, M.; Myers, J.N.; Stafford, R.J.; et al. Selective Uptake and Imaging of Aptamer- and Antibody-Conjugated Hollow Nanospheres Targeted to Epidermal Growth Factor Receptors Overexpressed in Head and Neck Cancer. *ACS Nano* **2014**, *8*, 4530–4538. [CrossRef]
184. Zhang, L.; Gao, S.; Zhang, F.; Yang, K.; Ma, Q.; Zhu, L. Activatable Hyaluronic Acid Nanoparticle as a Theranostic Agent for Optical/Photoacoustic Image-Guided Photothermal Therapy. *ACS Nano* **2014**, *8*, 12250–12258. [CrossRef] [PubMed]
185. Yin, W.; Yan, L.; Yu, J.; Tian, G.; Zhou, L.; Zheng, X.; Zhang, X.; Yong, Y.; Li, J.; Gu, Z.; et al. High-Throughput Synthesis of Single-Layer MoS2 Nanosheets as a Near-Infrared Photothermal-Triggered Drug Delivery for Effective Cancer Therapy. *ACS Nano* **2014**, *8*, 6922–6933. [CrossRef]
186. Vigderman, L.; Zubarev, E.R. Therapeutic platforms based on gold nanoparticles and their covalent conjugates with drug molecules. *Adv. Drug Delivery Rev.* **2013**, *65*, 663–676. [CrossRef]
187. Chen, Y.; Tan, C.; Zhang, H.; Wang, L. Two-dimensional graphene analogues for biomedical applications. *Chem. Soc. Rev.* **2015**, *44*, 2681–2701. [CrossRef] [PubMed]
188. Marquez, D.T.; Scaiano, J.C. Visible and Near-Infrared Plasmon-Mediated Molecular Release from Cucurbit[6]uril Mesoporous Gated Systems. *Langmuir* **2016**, *32*, 13764–13770. [CrossRef]
189. An, X.; Zhang, F.; Zhu, Y.; Shen, W. Photoinduced drug release from thermosensitive AuNPs-liposome using a AuNPs-switch. *Chem. Commun.* **2010**, *46*, 7202–7204. [CrossRef] [PubMed]
190. Geng, S.; Wu, L.; Cui, H.; Tan, W.; Chen, T.; Chu, P.K.; Yu, X.-F. Synthesis of lipid–black phosphorus quantum dot bilayer vesicles for near-infrared-controlled drug release. *Chem. Commun.* **2018**, *54*, 6060–6063. [CrossRef] [PubMed]
191. Takahashi, H.; Niidome, Y.; Yamada, S. Controlled release of plasmid DNA from gold nanorods induced by pulsed near-infrared light. *Chem. Commun.* **2005**, 2247–2249. [CrossRef]
192. Song, J.; Yang, X.; Jacobson, O.; Lin, L.; Huang, P.; Niu, G.; Ma, Q.; Chen, X. Sequential Drug Release and Enhanced Photothermal and Photoacoustic Effect of Hybrid Reduced Graphene Oxide-Loaded Ultrasmall Gold Nanorod Vesicles for Cancer Therapy. *ACS Nano* **2015**, *9*, 9199–9209. [CrossRef]
193. He, J.; Zhang, P.; Babu, T.; Liu, Y.; Gong, J.; Nie, Z. Near-infrared light-responsive vesicles of Au nanoflowers. *Chem. Commun.* **2013**, *49*, 576–578. [CrossRef]
194. Ding, Y.; Du, C.; Qian, J.; Dong, C.-M. NIR-Responsive Polypeptide Nanocomposite Generates NO Gas, Mild Photothermia, and Chemotherapy to Reverse Multidrug-Resistant Cancer. *Nano Lett.* **2019**, *19*, 4362–4370. [CrossRef]

195. Li, Y.; Deng, Y.; Tian, X.; Ke, H.; Guo, M.; Zhu, A.; Yang, T.; Guo, Z.; Ge, Z.; Yang, X.; et al. Multipronged Design of Light-Triggered Nanoparticles To Overcome Cisplatin Resistance for Efficient Ablation of Resistant Tumor. *ACS Nano* **2015**, *9*, 9626–9637. [CrossRef] [PubMed]
196. Zheng, M.; Yue, C.; Ma, Y.; Gong, P.; Zhao, P.; Zheng, C.; Sheng, Z.; Zhang, P.; Wang, Z.; Cai, L. Single-Step Assembly of DOX/ICG Loaded Lipid–Polymer Nanoparticles for Highly Effective Chemo-photothermal Combination Therapy. *ACS Nano* **2013**, *7*, 2056–2067. [CrossRef] [PubMed]
197. Wang, W.; Liang, G.; Zhang, W.; Xing, D.; Hu, X. Cascade-Promoted Photo-Chemotherapy against Resistant Cancers by Enzyme-Responsive Polyprodrug Nanoplatforms. *Chem. Mater.* **2018**, *30*, 3486–3498. [CrossRef]
198. Wang, W.; Satyavolu, N.S.R.; Wu, Z.; Zhang, J.-R.; Zhu, J.-J.; Lu, Y. Near-Infrared Photothermally Activated DNAzyme–Gold Nanoshells for Imaging Metal Ions in Living Cells. *Angew. Chem. Int. Ed.* **2017**, *56*, 6798–6802. [CrossRef]
199. Jeong, E.H.; Ryu, J.H.; Jeong, H.; Jang, B.; Lee, H.Y.; Hong, S.; Lee, H.; Lee, H. Efficient delivery of siRNAs by a photothermal approach using plant flavonoid-inspired gold nanoshells. *Chem. Commun.* **2014**, *50*, 13388–13390. [CrossRef]
200. Zhang, L.; Su, H.; Cai, J.; Cheng, D.; Ma, Y.; Zhang, J.; Zhou, C.; Liu, S.; Shi, H.; Zhang, Y.; et al. A Multifunctional Platform for Tumor Angiogenesis-Targeted Chemo-Thermal Therapy Using Polydopamine-Coated Gold Nanorods. *ACS Nano* **2016**, *10*, 10404–10417. [CrossRef]
201. Parchur, A.K.; Sharma, G.; Jagtap, J.M.; Gogineni, V.R.; LaViolette, P.S.; Flister, M.J.; White, S.B.; Joshi, A. Vascular Interventional Radiology-Guided Photothermal Therapy of Colorectal Cancer Liver Metastasis with Theranostic Gold Nanorods. *ACS Nano* **2018**, *12*, 6597–6611. [CrossRef]
202. Lin, L.-S.; Cong, Z.-X.; Cao, J.-B.; Ke, K.-M.; Peng, Q.-L.; Gao, J.; Yang, H.-H.; Liu, G.; Chen, X. Multifunctional Fe3O4@Polydopamine Core–Shell Nanocomposites for Intracellular mRNA Detection and Imaging-Guided Photothermal Therapy. *ACS Nano* **2014**, *8*, 3876–3883. [CrossRef]
203. Jc Bose, R.; Uday Kumar, S.; Zeng, Y.; Afjei, R.; Robinson, E.; Lau, K.; Bermudez, A.; Habte, F.; Pitteri, S.J.; Sinclair, R.; et al. Tumor Cell-Derived Extracellular Vesicle-Coated Nanocarriers: An Efficient Theranostic Platform for the Cancer-Specific Delivery of Anti-miR-21 and Imaging Agents. *ACS Nano* **2018**, *12*, 10817–10832. [CrossRef]
204. Zhong, J.; Yang, S.; Wen, L.; Xing, D. Imaging-guided photoacoustic drug release and synergistic chemo-photoacoustic therapy with paclitaxel-containing nanoparticles. *J. Control. Release* **2016**, *226*, 77–87. [CrossRef]
205. Liu, T.; Shi, S.; Liang, C.; Shen, S.; Cheng, L.; Wang, C.; Song, X.; Goel, S.; Barnhart, T.E.; Cai, W.; et al. Iron Oxide Decorated MoS2 Nanosheets with Double PEGylation for Chelator-Free Radiolabeling and Multimodal Imaging Guided Photothermal Therapy. *ACS Nano* **2015**, *9*, 950–960. [CrossRef] [PubMed]
206. Tomitaka, A.; Arami, H.; Huang, Z.; Raymond, A.; Rodriguez, E.; Cai, Y.; Febo, M.; Takemura, Y.; Nair, M. Hybrid magneto-plasmonic liposomes for multimodal image-guided and brain-targeted HIV treatment. *Nanoscale* **2018**, *10*, 184–194. [CrossRef] [PubMed]
207. Dong, L.; Zhang, P.; Xu, X.; Lei, P.; Du, K.; Zhang, M.; Wang, D.; Feng, J.; Li, W.; Zhang, H. Simple construction of Cu2−xS:Pt nanoparticles as nanotheranostic agent for imaging-guided chemo-photothermal synergistic therapy of cancer. *Nanoscale* **2018**, *10*, 10945–10951. [CrossRef] [PubMed]
208. Li, Z.; Liu, J.; Hu, Y.; Howard, K.A.; Li, Z.; Fan, X.; Chang, M.; Sun, Y.; Besenbacher, F.; Chen, C.; et al. Multimodal Imaging-Guided Antitumor Photothermal Therapy and Drug Delivery Using Bismuth Selenide Spherical Sponge. *ACS Nano* **2016**, *10*, 9646–9658. [CrossRef]
209. Pimlott, S.L.; Sutherland, A. Molecular tracers for the PET and SPECT imaging of disease. *Chem. Soc. Rev.* **2011**, *40*, 149–162. [CrossRef]
210. Sun, X.; Huang, X.; Yan, X.; Wang, Y.; Guo, J.; Jacobson, O.; Liu, D.; Szajek, L.P.; Zhu, W.; Niu, G.; et al. Chelator-Free 64Cu-Integrated Gold Nanomaterials for Positron Emission Tomography Imaging Guided Photothermal Cancer Therapy. *ACS Nano* **2014**, *8*, 8438–8446. [CrossRef]
211. Cheng, L.; Kamkaew, A.; Sun, H.; Jiang, D.; Valdovinos, H.F.; Gong, H.; England, C.G.; Goel, S.; Barnhart, T.E.; Cai, W. Dual-Modality Positron Emission Tomography/Optical Image-Guided Photodynamic Cancer Therapy with Chlorin e6-Containing Nanomicelles. *ACS Nano* **2016**, *10*, 7721–7730. [CrossRef]
212. Pang, B.; Zhao, Y.; Luehmann, H.; Yang, X.; Detering, L.; You, M.; Zhang, C.; Zhang, L.; Li, Z.-Y.; Ren, Q.; et al. 64Cu-Doped PdCu@Au Tripods: A Multifunctional Nanomaterial for Positron Emission Tomography and Image-Guided Photothermal Cancer Treatment. *ACS Nano* **2016**, *10*, 3121–3131. [CrossRef]

213. Chen, F.; Hong, H.; Zhang, Y.; Valdovinos, H.F.; Shi, S.; Kwon, G.S.; Theuer, C.P.; Barnhart, T.E.; Cai, W. In Vivo Tumor Targeting and Image-Guided Drug Delivery with Antibody-Conjugated, Radiolabeled Mesoporous Silica Nanoparticles. *ACS Nano* **2013**, *7*, 9027–9039. [CrossRef]
214. Zhou, M.; Li, J.; Liang, S.; Sood, A.K.; Liang, D.; Li, C. CuS Nanodots with Ultrahigh Efficient Renal Clearance for Positron Emission Tomography Imaging and Image-Guided Photothermal Therapy. *ACS Nano* **2015**, *9*, 7085–7096. [CrossRef] [PubMed]
215. Peng, C.-L.; Shih, Y.-H.; Lee, P.-C.; Hsieh, T.M.-H.; Luo, T.-Y.; Shieh, M.-J. Multimodal Image-Guided Photothermal Therapy Mediated by 188Re-Labeled Micelles Containing a Cyanine-Type Photosensitizer. *ACS Nano* **2011**, *5*, 5594–5607. [CrossRef] [PubMed]
216. Li, T.; Zhou, J.; Zhang, C.; Zhi, X.; Niu, J.; Fu, H.; Song, J.; Cui, D. Surface-engineered nanobubbles with pH-/light-responsive drug release and charge-switchable behaviors for active NIR/MR/US imaging-guided tumor therapy. *NPG Asia Mater.* **2018**, *10*, 1046–1060. [CrossRef]
217. de Smet, M.; Heijman, E.; Langereis, S.; Hijnen, N.M.; Grüll, H. Magnetic resonance imaging of high intensity focused ultrasound mediated drug delivery from temperature-sensitive liposomes: An in vivo proof-of-concept study. *J. Control. Release* **2011**, *150*, 102–110. [CrossRef]
218. Hijnen, N.; Kneepkens, E.; de Smet, M.; Langereis, S.; Heijman, E.; Grüll, H. Thermal combination therapies for local drug delivery by magnetic resonance-guided high-intensity focused ultrasound. *Proc. Natl. Acad. Sci. USA* **2017**, *114*, E4802–E4811. [CrossRef]
219. Izadifar, Z.; Izadifar, Z.; Chapman, D.; Babyn, P. An Introduction to High Intensity Focused Ultrasound: Systematic Review on Principles, Devices, and Clinical Applications. *J. Clin. Med.* **2020**, *9*, 460. [CrossRef]
220. Yoon, Y.I.; Pang, X.; Jung, S.; Zhang, G.; Kong, M.; Liu, G.; Chen, X. Smart gold nanoparticle-stabilized ultrasound microbubbles as cancer theranostics. *J. Mater. Chem. B* **2018**, *6*, 3235–3239. [CrossRef]
221. Liu, Y.; Yang, F.; Yuan, C.; Li, M.; Wang, T.; Chen, B.; Jin, J.; Zhao, P.; Tong, J.; Luo, S.; et al. Magnetic Nanoliposomes as in Situ Microbubble Bombers for Multimodality Image-Guided Cancer Theranostics. *ACS Nano* **2017**, *11*, 1509–1519. [CrossRef]
222. Lee, J.Y.; Carugo, D.; Crake, C.; Owen, J.; de Saint Victor, M.; Seth, A.; Coussios, C.; Stride, E. Nanoparticle-Loaded Protein–Polymer Nanodroplets for Improved Stability and Conversion Efficiency in Ultrasound Imaging and Drug Delivery. *Adv. Mater.* **2015**, *27*, 5484–5492. [CrossRef]
223. Jin, Z.; Wen, Y.; Hu, Y.; Chen, W.; Zheng, X.; Guo, W.; Wang, T.; Qian, Z.; Su, B.-L.; He, Q. MRI-guided and ultrasound-triggered release of NO by advanced nanomedicine. *Nanoscale* **2017**, *9*, 3637–3645. [CrossRef]
224. Zhang, L.; Yin, T.; Li, B.; Zheng, R.; Qiu, C.; Lam, K.S.; Zhang, Q.; Shuai, X. Size-Modulable Nanoprobe for High-Performance Ultrasound Imaging and Drug Delivery against Cancer. *ACS Nano* **2018**, *12*, 3449–3460. [CrossRef] [PubMed]
225. Shi, J.; Ma, Y.; Zhu, J.; Chen, Y.; Sun, Y.; Yao, Y.; Yang, Z.; Xie, J. A Review on Electroporation-Based Intracellular Delivery. *Molecules* **2018**, *23*, 3044. [CrossRef] [PubMed]
226. Gao, K.; Li, L.; He, L.; Hinkle, K.; Wu, Y.; Ma, J.; Chang, L.; Zhao, X.; Perez, D.G.; Eckardt, S.; et al. Design of a Microchannel-Nanochannel-Microchannel Array Based Nanoelectroporation System for Precise Gene Transfection. *Small* **2014**, *10*, 1015–1023. [CrossRef]
227. Mouli, S.K.; Tyler, P.; McDevitt, J.L.; Eifler, A.C.; Guo, Y.; Nicolai, J.; Lewandowski, R.J.; Li, W.; Procissi, D.; Ryu, R.K.; et al. Image-Guided Local Delivery Strategies Enhance Therapeutic Nanoparticle Uptake in Solid Tumors. *ACS Nano* **2013**, *7*, 7724–7733. [CrossRef]
228. Ruiz-Hernández, E.; Baeza, A.; Vallet-Regí, M. Smart Drug Delivery through DNA/Magnetic Nanoparticle Gates. *ACS Nano* **2011**, *5*, 1259–1266. [CrossRef]
229. Dunn, A.E.; Dunn, D.J.; Macmillan, A.; Whan, R.; Stait-Gardner, T.; Price, W.S.; Lim, M.; Boyer, C. Spatial and temporal control of drug release through pH and alternating magnetic field induced breakage of Schiff base bonds. *Polym. Chem.* **2014**, *5*, 3311–3315. [CrossRef]
230. Tay, Z.W.; Chandrasekharan, P.; Chiu-Lam, A.; Hensley, D.W.; Dhavalikar, R.; Zhou, X.Y.; Yu, E.Y.; Goodwill, P.W.; Zheng, B.; Rinaldi, C.; et al. Magnetic Particle Imaging-Guided Heating in Vivo Using Gradient Fields for Arbitrary Localization of Magnetic Hyperthermia Therapy. *ACS Nano* **2018**, *12*, 3699–3713. [CrossRef]
231. Liu, J.F.; Neel, N.; Dang, P.; Lamb, M.; McKenna, J.; Rodgers, L.; Litt, B.; Cheng, Z.; Tsourkas, A.; Issadore, D. Radiofrequency-Triggered Drug Release from Nanoliposomes with Millimeter-Scale Resolution Using a Superimposed Static Gating Field. *Small* **2018**, *14*, 1802563. [CrossRef]

232. Fuller, E.G.; Sun, H.; Dhavalikar, R.D.; Unni, M.; Scheutz, G.M.; Sumerlin, B.S.; Rinaldi, C. Externally Triggered Heat and Drug Release from Magnetically Controlled Nanocarriers. *ACS Appl. Mater. Interfaces* **2019**, *1*, 211–220. [CrossRef]
233. Xu, X.; Hou, S.; Wattanatorn, N.; Wang, F.; Yang, Q.; Zhao, C.; Yu, X.; Tseng, H.-R.; Jonas, S.J.; Weiss, P.S. Precision-Guided Nanospears for Targeted and High-Throughput Intracellular Gene Delivery. *ACS Nano* **2018**, *12*, 4503–4511. [CrossRef]
234. Maeda, H. The enhanced permeability and retention (EPR) effect in tumor vasculature: The key role of tumor-selective macromolecular drug targeting. *Adv. Enzyme Regul.* **2001**, *41*, 189–207. [CrossRef]
235. Low, P.S.; Henne, W.A.; Doorneweerd, D.D. Discovery and Development of Folic-Acid-Based Receptor Targeting for Imaging and Therapy of Cancer and Inflammatory Diseases. *Acc. Chem. Res.* **2008**, *41*, 120–129. [CrossRef] [PubMed]
236. Kamaly, N.; Xiao, Z.; Valencia, P.M.; Radovic-Moreno, A.F.; Farokhzad, O.C. Targeted polymeric therapeutic nanoparticles: Design, development and clinical translation. *Chem. Soc. Rev.* **2012**, *41*, 2971–3010. [CrossRef] [PubMed]
237. Gianella, A.; Jarzyna, P.A.; Mani, V.; Ramachandran, S.; Calcagno, C.; Tang, J.; Kann, B.; Dijk, W.J.R.; Thijssen, V.L.; Griffioen, A.W.; et al. Multifunctional Nanoemulsion Platform for Imaging Guided Therapy Evaluated in Experimental Cancer. *ACS Nano* **2011**, *5*, 4422–4433. [CrossRef] [PubMed]
238. Kunjachan, S.; Pola, R.; Gremse, F.; Theek, B.; Ehling, J.; Moeckel, D.; Hermanns-Sachweh, B.; Pechar, M.; Ulbrich, K.; Hennink, W.E.; et al. Passive versus Active Tumor Targeting Using RGD- and NGR-Modified Polymeric Nanomedicines. *Nano Lett.* **2014**, *14*, 972–981. [CrossRef] [PubMed]
239. Chen, Y.; Foss, C.A.; Byun, Y.; Nimmagadda, S.; Pullambhatla, M.; Fox, J.J.; Castanares, M.; Lupold, S.E.; Babich, J.W.; Mease, R.C.; et al. Radiohalogenated Prostate-Specific Membrane Antigen (PSMA)-Based Ureas as Imaging Agents for Prostate Cancer. *J. Med. Chem.* **2008**, *51*, 7933–7943. [CrossRef]
240. Shukla, R.; Thomas, T.P.; Desai, A.M.; Kotlyar, A.; Park, S.J.; Baker, J.R., Jr. HER2 specific delivery of methotrexate by dendrimer conjugated anti-HER2 mAb. *Nanotechnology* **2008**, *19*, 295102. [CrossRef]
241. Thomas, T.P.; Choi, S.K.; Li, M.-H.; Kotlyar, A.; Baker, J.R., Jr. Design of Riboflavin-Presenting PAMAM Dendrimers as a New Nanoplatform for Cancer-Targeted Delivery. *Bioorg. Med. Chem. Lett.* **2010**, *20*, 5191–5194. [CrossRef]
242. Plantinga, A.; Witte, A.; Li, M.-H.; Harmon, A.; Choi, S.K.; Banaszak Holl, M.M.; Orr, B.G.; Baker, J.R., Jr.; Sinniah, K. Bioanalytical Screening of Riboflavin Antagonists for Targeted Drug Delivery—A Thermodynamic and Kinetic Study. *ACS Med. Chem. Lett.* **2011**, *2*, 363–367. [CrossRef]
243. Qian, Z.M.; Li, H.; Sun, H.; Ho, K. Targeted Drug Delivery via the Transferrin Receptor-Mediated Endocytosis Pathway. *Pharmacol. Rev.* **2002**, *54*, 561–587. [CrossRef]
244. He, H.; Liu, L.; Morin, E.E.; Liu, M.; Schwendeman, A. Survey of Clinical Translation of Cancer Nanomedicines—Lessons Learned from Successes and Failures. *Acc. Chem. Res.* **2019**, *52*, 2445–2461. [CrossRef] [PubMed]
245. Sartor, O. Eligard: Leuprolide acetate in a novel sustained-release delivery system. *Urology* **2003**, *61*, 25–31. [CrossRef]
246. Sparreboom, A.; Scripture, C.D.; Trieu, V.; Williams, P.J.; De, T.; Yang, A.; Beals, B.; Figg, W.D.; Hawkins, M.; Desai, N. Comparative Preclinical and Clinical Pharmacokinetics of a Cremophor-Free, Nanoparticle Albumin-Bound Paclitaxel (ABI-007) and Paclitaxel Formulated in Cremophor (Taxol). *Clin. Cancer Res.* **2005**, *11*, 4136–4143. [CrossRef] [PubMed]
247. Lyass, O.; Uziely, B.; Ben-Yosef, R.; Tzemach, D.; Heshing, N.I.; Lotem, M.; Brufman, G.; Gabizon, A. Correlation of toxicity with pharmacokinetics of pegylated liposomal doxorubicin (Doxil) in metastatic breast carcinoma. *Cancer* **2000**, *89*, 1037–1047. [CrossRef]
248. Venkatakrishnan, K.; Liu, Y.; Noe, D.; Mertz, J.; Bargfrede, M.; Marbury, T.; Farbakhsh, K.; Oliva, C.; Milton, A. Pharmacokinetics and pharmacodynamics of liposomal mifamurtide in adult volunteers with mild or moderate hepatic impairment. *Br. J. Clin. Pharmacol.* **2014**, *77*, 998–1010. [CrossRef]
249. Silverman, J.A.; Deitcher, S.R. Marqibo® (vincristine sulfate liposome injection) improves the pharmacokinetics and pharmacodynamics of vincristine. *Cancer Chemother. Pharmacol.* **2013**, *71*, 555–564. [CrossRef]
250. Zhang, H. Onivyde for the therapy of multiple solid tumors. *OncoTargets Ther.* **2016**, *9*, 3001–3007. [CrossRef]

251. Dunne, M.; Epp-Ducharme, B.; Sofias, A.M.; Regenold, M.; Dubins, D.N.; Allen, C. Heat-activated drug delivery increases tumor accumulation of synergistic chemotherapies. *J. Control. Release* **2019**, *308*, 197–208. [CrossRef]
252. Huggett, M.T.; Jermyn, M.; Gillams, A.; Illing, R.; Mosse, S.; Novelli, M.; Kent, E.; Bown, S.G.; Hasan, T.; Pogue, B.W.; et al. Phase I/II study of verteporfin photodynamic therapy in locally advanced pancreatic cancer. *Br. J. Cancer* **2014**, *110*, 1698–1704. [CrossRef]
253. Obaid, G.; Broekgaarden, M.; Bulin, A.-L.; Huang, H.-C.; Kuriakose, J.; Liu, J.; Hasan, T. Photonanomedicine: A convergence of photodynamic therapy and nanotechnology. *Nanoscale* **2016**, *8*, 12471–12503. [CrossRef]
254. Maisch, T.; Santarelli, F.; Schreml, S.; Babilas, P.; Szeimies, R.-M. Fluorescence induction of protoporphyrin IX by a new 5-aminolevulinic acid nanoemulsion used for photodynamic therapy in a full-thickness ex vivo skin model. *Exp. Dermatol.* **2010**, *19*, e302–e305. [CrossRef] [PubMed]
255. de Bruijn, H.S.; Brooks, S.; van der Ploeg-van den Heuvel, A.; ten Hagen, T.L.M.; de Haas, E.R.M.; Robinson, D.J. Light Fractionation Significantly Increases the Efficacy of Photodynamic Therapy Using BF-200 ALA in Normal Mouse Skin. *PLoS ONE* **2016**, *11*, e0148850. [CrossRef] [PubMed]